EUROPEAN ORGANIZATION FOR NUCLEAR RESEARCH

CERN/PPE 91-40
20 February 1991

STUDY OF THE CENTRALLY PRODUCED $\pi\pi$ AND $K\bar{K}$ SYSTEMS AT 85 AND 300 GeV/c

WA76 Collaboration
Athens-Bari-Birmingham-CERN-Collège de France

T.A. Armstrong[4a], M. Benayoun[5], W. Beusch[4], I.J. Bloodworth[3], J.N. Carney[3], R. Childs[3], C. Evangelista[2], B.R. French[4], B. Ghidini[2], M. Girone[2], A. Jacholkowski[4], J. Kahane[5], J.B. Kinson[3], A. Kirk[4], K. Knudson[4], V. Lenti[2], Ph. Leruste[5], A. Malamant[5], J.L. Narjoux[5], F. Navach[2], A. Palano[2], E. Quercigh[4], N. Redaelli[4b] L. Rossi[4c], M. Sené[5], R. Sené[5], M. Stassinaki[1], M.T. Trainor[3d], G. Vassiliadis[1], O. Villalobos Baillie[3] and M.F. Votruba[3]

3 1 7

Abstract

We have studied the $\pi\pi$ and $K\bar{K}$ systems centrally produced in proton proton collisions at 300 GeV/c and π^+/p proton collisions at 85 GeV/c using the CERN Ω spectrometer. Clear evidence for $S^*/f_0(975)$ production is observed. An analysis performed on the $\pi^+\pi^-$ mass spectrum in the 1.0 GeV region, using a coupled channel formalism, shows that it is possible to describe the $S^*/f_0(975)$ effect with one single resonance once interference of the $S^*/f_0(975)$ with the S-wave background is introduced. The resulting $S^*/f_0(975)$ parameters are $m_0 = 979 \pm 4$ MeV, $g_\pi = 0.28 \pm 0.04$, $g_K = 0.56 \pm 0.18$ corresponding to a pole position on sheet II at $(1001 \pm 2) - i(36 \pm 4)$ MeV. Evidence is also found for a structure having a mass of 1472 ± 12 MeV and a width of 195 ± 33 MeV.

Submitted to Zeitschrift für Physik C

---

1) Athens University, Nuclear Physics Department, Athens, Greece
2) Dipartimento di Fisica dell'Università and Sezione INFN, Bari, Italy
3) University of Birmingham, Physics Department, Birmingham, U.K.
4) CERN, European Organization for Nuclear Research, Geneva, Switzerland
5) Collège de France, Paris, France
a) Present address: Pennsylvania State University, University Park, USA
b) Present address: INFN and Dipartimento di Fisica, Milan, Italy
c) Present address: INFN and Dipartimento di Fisica, Genoa, Italy
d) Now at Oxford University, Oxford, U.K.

1. INTRODUCTION

The understanding of meson spectroscopy is of fundamental importance in the search for gluonium or hybrid states which are expected, from QCD, to populate the low mass region of the hadron spectrum. Two gluonium candidates already exist: the $J^{PC} = 0^{-+}$ $\iota/\eta(1440)$ observed in J/ψ decay [1] and the $J^{PC} = 2^{++}$ $\theta/f_2(1720)$ observed in J/ψ decay [2,3,4] and central production [5]. Several theoretical models predict the $J^{PC} = 0^{++}$ glueball to be the lightest and to lie in the mass region between 1.0 and 1.5 GeV [6]. However, the present situation of light-meson spectroscopy is rather confused in this mass range. For this reason it is now clear that the discovery of gluonium states can only come from the comparison of resonance production from different mechanisms, i.e. J/ψ decay, central production, $\gamma\gamma$ collisions, $p\bar{p}$ annihilation and peripheral reactions.

The search for narrow scalar mesons below 1.4 GeV has been carried out in a study of radiative decay of J/ψ to $\pi\pi$ and $K\bar{K}$, with negative results [7]. There still exists, however, an unexplained structure around 1.45 GeV in the radiative decay of the J/ψ to $\pi\pi$ [8]. The hadronic decay of the J/ψ, on the other hand, shows good evidence for $S^*/f_0(975)$ production in the $\pi^+\pi^-$ mass spectrum recoiling against $\phi(1020)$ and somewhat weaker evidence when recoiling against the $\omega(783)$. An unexplained structure is also visible in the 1.4 GeV region of the $\pi^+\pi^-$ mass spectrum opposite the $\phi(1020)$ for which a scalar contribution seems to be present [9].

High statistics studies with incident pions [10] of the I = 0, $J^{PC} = 0^{++}$ $\pi^+\pi^-$ system lead to the conclusion that a broad $\epsilon/f_0(1400)$ and a narrow $S^*/f_0(975)$ exist. Weak evidence for the production of the $S^*/f_0(975)$ in $\gamma\gamma$ collisions has been reported [11]. Evidence for the $S^*/f_0(975)$ has also been found in the decay $D_s \rightarrow S^*/f_0(975)\pi$ where $S^*/f_0(975) \rightarrow \pi^+\pi^-$ [12]. The above results suggest a substantial $s\bar{s}$ component in the $S^*/f_0(975)$ wavefunction. A recent analysis [13] of central dipion production [14] indicates a different scenario: the $S^*/f_0(975)$ is a gluonium state while an $s\bar{s}$ scalar resonance may be present in the threshold region of the $K\bar{K}$ spectrum. There are also suggestions that the $S^*/f_0(975)$ could be a 4-quark state [15] or a $K\bar{K}$ molecule [16]. A particular property of the $S^*/f_0(975)$ is that it often appears as a sharp drop in the $\pi^+\pi^-$ mass spectrum and only in a few cases as a narrow peak.

In this paper we describe the results from a search for gluonium states in the centrally produced $\pi\pi$ and $K\bar{K}$ final states by using data from two different runs of the WA76 experiment performed at the CERN Ω spectrometer. The first run studied the reactions

$$\pi^+ p \rightarrow \pi_f^+(X^0)p_s \tag{1}$$

and

$$pp \rightarrow p_f(X^0)p_s \tag{2}$$

using an 85 GeV/c incident beam momentum. The second run studied reaction (2) only with an incident beam momentum of 300 GeV/c. This paper begins by showing the results coming from the 300 GeV/c run, which gave the higher statistics data on the $\pi\pi$ final state, and then we compare these results with those coming from the 85 GeV/c run. Details of

the layout of the apparatus, trigger conditions and data processing for the two experiments have been given in previous publications [17,18].

2. STUDY OF THE $\pi^+\pi^-$ SYSTEM AT 300 GeV/c

The reaction

$$pp \rightarrow p_f(\pi^+\pi^-)p_s \tag{3}$$

has been selected from the sample of 4-prong events by requiring momentum balance, i.e. |missing P_x| < 20 GeV/c, |missing P_y| < 0.16 GeV/c and |missing P_z| < 0.08 GeV/c. The energy balance was ensured by requiring the Ehrlich mass squared [19] (shown in fig. 1(a)) to be in the range from -0.14 to 0.16 GeV^2. Events having one of the central particles identified by the Cherenkov system as a K, p or ambiguous K/p (for which the Ehrlich mass squared is shown in fig. 1(b), have been removed. Events where the slow particle was identified as a π^+ using a pulse height momentum correlation, have also been removed. The trigger of the present experiment was set up in order to antiselect forward or backward diffractive contributions. The $p_f\pi^+$ effective mass (fig. 2(a)) shows evidence for a residual Δ^{++} signal which has been removed by requiring the centre of mass rapidity of the π^+ to be smaller than 1.6. The $p_s\pi^+$ effective mass (fig. 2(c)), on the other hand, shows no Δ^{++} signal. Resonance structures in the $p\pi^-$ mass distributions (fig. 2(b,d)) are rather weak. The final sample consists of 302 619 events whose $\pi^+\pi^-$ effective mass spectrum is shown in fig. 3. We observe a small $\rho(770)$ signal, some $f_2(1270)$ and a sharp drop around 1 GeV. The Feynman-x_F distributions for the slow proton, the central dipion system and the fast proton are shown in fig. 4.

3. A FIT TO THE $\pi^+\pi^-$ MASS SPECTRUM

In order to extract the $S^*/f_0(975)$ parameters, a fit to the $\pi^+\pi^-$ mass spectrum has been performed using relativistic P and D wave Breit–Wigner formulae to describe the $\rho(770)$ and $f_2(1270)$ and a coupled channel Breit–Wigner [20] to describe the $S^*/f_0(975)$ region.

Taking $\sqrt{\Gamma}_i$ to be the coupling of the exchanged particles to the X^0 system, $\sqrt{\Gamma}_\pi$ and $\sqrt{\Gamma}_K$ to describe the couplings of the X^0 system to the $\pi\pi$ and $K\bar{K}$ final states respectively and neglecting final state interaction effects, we have written the coupled channel Breit–Wigner which describes the $S^*/f_0(975)$ resonance as

$$F_\pi(m) = \frac{m_0\sqrt{\Gamma}_i\sqrt{\Gamma}_\pi}{m_0^2 - m^2 - im_0(\Gamma_\pi + \Gamma_K)} \tag{4}$$

in the $\pi\pi$ channel and

$$F_K(m) = \frac{m_0\sqrt{\Gamma}_i\sqrt{\Gamma}_K}{m_0^2 - m^2 - im_0(\Gamma_\pi + \Gamma_K)} \tag{5}$$

in the $K\bar{K}$ channel. The value of Γ_i is unknown and has been absorbed into the intensity of the resonance. Γ_π and Γ_K describe the $S^*/f_0(975)$ partial widths to $\pi\pi$ and $K\bar{K}$

$$\Gamma_\pi = g_\pi(m^2/4 - m_\pi^2)^{1/2} \quad ,$$

$$\Gamma_K = g_K/2[(m^2/4 - m_{K^+}^2)^{1/2} + (m^2/4 - m_{K^0}^2)^{1/2}] \quad ,$$

where g_π and g_K are the squares of the couplings of $S^*/f_0(975)$ to $\pi\pi$ and $K\bar{K}$ systems.

The background has been parametrized as

$$G(m) = (m - m_{th})^\alpha \quad e^{-\beta m - \gamma m^2} \quad , \tag{6}$$

where m_{th} is the $\pi\pi$ threshold mass. Inserting incoherently the $F_\pi(m)$ in the fit gives a poor description of the data. In order to have a satisfactory description of the $S^*/f_0(975)$ region it was found necessary to introduce an interference between the coupled channel Breit–Wigner $F_\pi(m)$ and the background. The S-wave contribution was parametrized as

$$B_s(m) = |1 + A_s F_\pi(m) e^{i\delta_1}|^2 \quad , \tag{7}$$

where δ_1 is a mass independent phase. In order to have a satisfactory fit in the low mass region around 0.5 GeV, it was also necessary to introduce an $\omega(783)$ reflection in the low mass region of the $\pi^+\pi^-$ mass spectrum. Some events from the $\pi^+\pi^-\pi^0$ final state have a slow π^0 with a small transverse momentum which falls inside the momentum balance cuts which define reaction (2). We have selected events belonging to the reaction

$$pp \rightarrow p_f(\pi^+\pi^-\pi^0)p_s$$

from the sample of events having two gammas detected in the electromagnetic calorimeter. Figure 5 shows the $\pi^+\pi^-\pi^0$ effective mass spectrum requiring the two gammas to come from a π^0 decay: above the η, a strong $\omega(783)$ can been seen. The $\omega(783)$ reflection in the $\pi^+\pi^-$ channel, $\omega(m)$, has been computed using a Monte Carlo simulation and included in the fit as a histogram whose amplitude was a free parameter.

The expression used for the fit to the $\pi^+\pi^-$ mass spectrum is the following:

$$dN/dm = \omega(m) + G(m)[B_s(m) + A_\rho B_\rho(m) + A_f B_f(m) + A_\theta B_\theta(m)]$$

where $B_\rho(m)$ and $B_f(m)$ represent the $\rho(770)$ and $f_2(1270)$ Breit–Wigner amplitudes having parameters fixed to the PDG values [21]. $B_\theta(m)$ represents the contribution of the $\theta/f_2(1720)$ which has been observed to decay to $\pi^+\pi^-$ [3], with mass and width set to the values from the fit of the K^+K^- mass spectrum of the present experiment [5]. The coupled channel Breit–Wigner used to describe the $S^*/f_0(975)$ resonance has been convoluted with a Gaussian representing the experimental resolution which has a σ of 10 MeV in the 1.0 GeV region. In this hypothesis the fit gives a good description of the data in the first part of the mass spectrum but fails to describe it in the 1.5 GeV region as can be seen from fig. 6(a).

Several attempts have been made to describe the 1.5 GeV mass region. We tried first an interference between the $f_2(1270)$ and a possible $\pi\pi$ decay mode of the $f_2'(1525)$ but this hypothesis did not improve the fit by a large amount. The inclusion of a new incoherent Breit–Wigner did not describe the data satisfactorily either. It was found that by introducing an interference between the $f_2(1270)$, $f_2'(1525)$ and the background the fit improved but the fit probability remained low (0.2%). In this hypothesis we measure a branching ratio $\Gamma(f_2' \rightarrow \pi\pi)/\Gamma(f_2' \rightarrow K\bar{K}) = 0.21 \pm 0.08$. If, however, we include a Breit–Wigner shape having free parameters and interfering with the background, i.e. by replacing (7) with the expression

$$B_s(m) = |1 + A_s F_\pi(m) e^{i\delta_1} + A_X F_X(m) e^{i\delta_2}|^2 \quad ,$$

the fit probability increases to 51% and we obtain

$$\begin{aligned} m_X &= 1472 \pm 12 \text{ MeV} \quad , \\ \Gamma_X &= 195 \pm 33 \text{ MeV} \quad , \\ \delta_2 &= 159 \pm 8^0 \quad , \end{aligned}$$

as parameters for this new Breit–Wigner. This structure may be related to the signal observed in radiative and hadronic J/ψ decay [8,9] and in π induced reactions [10]. The result from this fit in the 1.5 GeV region is shown in fig. 6(b). The resulting $S^*/f_0(975)$ parameters are

$$\begin{aligned} m_0 &= 979 \pm 4 \quad \text{MeV} \quad , \\ g_\pi &= 0.28 \pm 0.04 \quad , \\ g_K &= 0.56 \pm 0.18 \quad , \\ \delta_1 &= 23 \pm 4^0 \quad , \end{aligned}$$

with a pole position on sheet II at $(1001 \pm 2) - i(36 \pm 4)$ MeV. The resonance full width is given by twice the imaginary part of the pole position resulting in $\Gamma_{S^*/f_0(975)} = 72 \pm 8$ MeV. The results of the fit are given in table I and shown, as a curve superimposed on the data, in fig. 7(a,b).

For the $\theta/f_2(1720)$ we measure a branching ratio

$$\frac{B(\theta/f_2(1720) \rightarrow \pi\pi)}{B(\theta/f_2(1720) \rightarrow K\overline{K})} = 0.39 \pm 0.14$$

consistent with that measured in radiative J/ψ decay [3].

We note that the g_K parameter which has been measured from the $\pi\pi$ data has a large error, despite the large statistics. We have tested the sensitivity of the data to this parameter by fixing g_K to zero and leaving all the fit parameters free. The fit probability in this case decreases from 51% to 4% thus still giving an acceptable description of the data. This is to be compared to the case where we put to zero the interference of the $S^*/f_0(975)$ Breit–Wigner with the background and found it impossible to obtain a reasonable fit to the data.

4. COMPARISON WITH THE K^+K^- DATA

Using the results from the fit of the $\pi^+\pi^-$ spectrum it is possible, by means of expression (5) and the intensity coming from the fit, to have an absolute prediction of the expected number of events for the $S^*/f_0(975)$ in the K^+K^- spectrum.

The reaction

$$pp \rightarrow p_f(K^+K^-)p_s$$

has been isolated from the sample of 4-prong events by first requiring momentum balance with the criteria used for reaction (3), then selecting events having one of the central particles identified by the Cherenkov system as K, p or ambiguous K/p, and finally requiring the Ehrlich mass squared (shown in fig. 1(b)) to be in the range 0.18 to 0.56 GeV^2. This leads to 6564 events, whose mass spectrum is shown in fig. 8(a). The requirement of the Cherenkov identification puts the K^+K^- system in a different kinematical configuration with respect to the $\pi^+\pi^-$ final state. The relative normalization between the $\pi^+\pi^-$ and K^+K^- spectra in the 1.0 GeV region has been estimated using two different methods. Firstly, we have computed the geometrical acceptance for the two channels. Since we are interested in the same mass region for both final states, we have not considered the contributions to the geometrical acceptance due to the fast and slow protons. We have then taken pions from different events, rotated them isotropically around the beam axis in the laboratory system and translated along the hydrogen target; finally the trigger conditions have been applied in the two hypotheses where the two tracks simulated the $\pi^+\pi^-$ or the K^+K^- final states. The resulting acceptances estimated by this method are shown in figs 9(a) and 9(b) as functions of the $\pi^+\pi^-$ and K^+K^- effective mass, respectively.

The second method made use of the presence of the $\phi(1020)$ signal. In order to estimate the loss of events in the 1.0 GeV region produced by the selection described above, we have produced a different unbiased K^+K^- spectrum, where only events having positively identified π's have been removed. This spectrum has a large $\pi^+\pi^-$ contamination as can be seen from fig. 10(a) where the Ehrlich mass is shown for this selection, but the narrow $\phi(1020)$ is still clearly visible (fig. 10(b)). By fitting the number of $\phi(1020)$ events in the two spectra we obtained an estimate of the change in geometrical acceptance introduced by the K identification in the 1.0 GeV region. The values given by the two methods have been found to be similar.

The contamination, in the K^+K^- channel, from the $\pi^+\pi^-$ channel where one pion has been misidentified as a K, has been estimated to be of the order of 10% by using the distribution shown in fig. 1(b). This contamination is shown in fig. 8(a) as a dashed histogram. By subtracting this contribution we obtain the K^+K^- effective mass spectrum shown in fig. 8(b). The black band drawn in the threshold region of fig. 8(b) represents the predicted $S^*/f_0(975)$ contribution after having taken into account the different geometrical acceptances of the two channels and Clebsch–Gordan coefficients. Function (5) has been convoluted with a Gaussian representing the experimental resolution which has a σ of 6 MeV in this mass region. The band shows the one-standard deviation limits of the prediction. Such a contribution is easily accommodated in the threshold region of the

K^+K^- mass spectrum.

5. COMPARISON WITH THE $K^0_SK^0_S$ DATA

It is interesting to compare the above result with the $K^0_SK^0_S$ mass spectrum. Although this channel suffers from low statistics, it has the advantage of not being complicated by the presence of the $\phi(1020)$ in the threshold region.

The reaction

$$pp \rightarrow p_f(K^0_SK^0_S)p_s$$

has been isolated from the sample of events having two reconstructed V^0s which balance momentum. In order to remove the background due to random $\pi^+\pi^-$ combinations, a decay length of at least 3 cm was required for each of the two V^0s. The $\pi^+\pi^-$ mass spectrum of the two V^0s, for the 300 GeV/c data, is shown in fig. 11(a) and reveals a clear K^0 signal over little background. Selecting events having the K^0 mass in the range 0.475 to 0.520 GeV produces the $K^0_SK^0_S$ mass spectrum shown in fig. 12 for the combined 85 and 300 GeV/c data. The $K^0_SK^0_S$ mass spectrum shows similar features to the K^+K^- mass spectrum, viz. a threshold enhancement, the $f'_2(1525)$ and the $\theta/f_2(1720)$. The curve drawn in the threshold region represents the $S^*/f_0(975)$ contribution to the $K^0_SK^0_S$ final state. The K^+K^- and $K^0_SK^0_S$ channels have been normalized to each other by firstly correcting the channels for the geometrical acceptance of the apparatus and for the losses due to the detection of two K^0s (shown in fig. 11(b)) and then by using the presence of the $f'_2(1525)$ seen in both mass spectra. It can be seen that the projected curve in fig. 12 can easily be accomodated in the threshold region of the $K^0_SK^0_S$ mass spectrum.

6. STUDY OF THE t DEPENDENCE

The uncorrected four-momentum transfer distributions $|t_1|$, $|t_2|$ and $t = |t_1 + t_2|$ (fig. 13(a)) for the double exchange graph for reaction (3) are shown in fig. 13(b,c,d) respectively. A depletion of events can be seen for small values of t_2 due to the loss of slow protons with momenta below 200 MeV/c.

We have studied the t dependence of the resonances observed in the $\pi^+\pi^-$ mass spectrum by dividing the data sample into two t regions. Figure 14(a,b) shows the $\pi^+\pi^-$ effective mass distributions for $t < 0.3$ GeV^2 and $t > 0.3$ GeV^2. In the high t region the presence of $S^*/f_0(975), \rho(770)$ and $f_2(1270)$ can be seen, while in the low t region the $\rho(770)$ and $f_2(1270)$ signals are suppressed. This observation is in agreement with previous measurements of centrally produced $\pi^+\pi^-$ mass spectra at ISR energies [14,22]. The data from ref. [14], produced at low t, show no signs of the $f_2(1270)$, while the data from ref. [22], at high t, show a strong $f_2(1270)$ signal.

In order to obtain a quantitative measurement of this effect we have performed fits to the $\pi^+\pi^-$ mass spectrum in different t regions, fixing the $S^*/f_0(975)$ parameters to the values obtained from the fit to the total mass spectrum but allowing the interference

phases δ_1 and δ_2 to vary. The $\pi^+\pi^-$ effective mass distributions in each of the t intervals are shown in fig. 15 together with the results from the fits. It can be seen that the description of the data is good in all cases, with fit probabilities which range between 23% and 89%. The values obtained for δ_1 and δ_2 as a function of t are plotted in fig. 16(a). The average geometrical acceptance of the apparatus as a function of t has been estimated by Monte Carlo simulation and is shown in fig. 16(b). The corrected and uncorrected t distributions for $S^*/f_0(975)$, $f_2(1270)$, $\rho(770)$ and X(1470) are shown in fig. 17.

It can be noticed that, while the $S^*/f_0(975)$ and X(1470) distributions behave like a simple exponential having slopes respectively 8.7 ± 0.2 GeV^{-2} and 11.2 ± 0.9 GeV^{-2}, the $\rho(770)$ and $f_2(1270)$ distributions are consistent with zero in the first t interval, suggesting a turnover at low t.

It is interesting to compare the t behaviour of the $f_2(1270)$ with that of the two other I = 0 tensors observed in the same experiment, the $f_2'(1525)$ and the $\theta/f_2(1720)$, in the K^+K^- channel. Figure 18 shows the K^+K^- effective mass distributions for $t < 0.3$ GeV^2 and $t > 0.3$ GeV^2. We observe enhanced production of $\theta/f_2(1720)$ at low t, in contrast with the behaviour of $f_2(1270)$ and $f_2'(1525)$. Thus, the data indicate a different production mechanism for the gluonium candidate $\theta/f_2(1720)$ with respect to the other two I = 0 tensors $f_2(1270)$ and $f_2'(1525)$, in the central Feynman-x_F region covered by this experiment, in agreement with the expectations for a tensor glueball [23]. By dividing the K^+K^- data into four regions of t and correcting for geometrical acceptance, we obtain the t distributions shown in fig. 19. Fitting them by simple exponentials we obtain slopes of 6.1 ± 0.4 GeV^{-2} and 9.6 ± 0.4 GeV^{-2}, respectively for the $f_2'(1525)$ and $\theta/f_2(1720)$.

In order to obtain the corresponding t behaviour for the $\phi(1020)$ the selection criteria described in sect. 4 have been used to maximize the available statistics. This can be done since the $\phi(1020)$ can be detected even in the presence of a substantial background. The K^+K^- effective mass distributions in the $\phi(1020)$ region for t < 0.3 GeV^2 and t > 0.3 GeV^2 are shown in fig. 20(a,b). Evidence for a suppression of the $\phi(1020)$ in the low t region can be seen. By dividing the data into four t regions the distribution shown in fig. 20(c) is obtained.

7. STUDY OF THE $\pi^0\pi^0$ FINAL STATE

The reaction

$$pp \rightarrow p_f(\pi^0\pi^0)p_s$$

has been selected from the sample of 2-prong events having four reconstructed γ's each with an energy greater than 1 GeV in the electromagnetic calorimeter. This energy cut was increased to 2.5 GeV in a 30 cm radius around the fast proton impact point on the γ calorimeter. Momentum balance was obtained by requiring |missing P_x| < 30 GeV/c, |missing P_y| < 0.16 GeV/c and |missing P_z| < 0.08 GeV/c . Figure 21 shows the scatter diagram $m(\gamma_1\gamma_2)$ vs $m(\gamma_3\gamma_4)$ (3 combinations per event) where a clear peak is visible at the position corresponding to the $\pi^0\pi^0$ channel. The $\gamma\gamma$ effective mass after having required the other $\gamma\gamma$ pair to lie in the π^0 region (0.1–0.18 GeV), is shown

in fig. 22(a). Selecting the two $\gamma\gamma$ combinations in the $\pi^0\pi^0$ region, the momenta of the $\gamma's$ have been fitted to the π^0 mass. The $p_f\pi^0$ effective mass distribution shows a strong Δ^+ (fig. 22(b)) which has been removed by requiring $m(p_f\pi^0) > 1.50$ GeV.

The remaining sample of 5578 central $\pi^0\pi^0$ events have a mass spectrum which is shown in fig. 23. The distribution shows a drop at the $S^*/f_0(975)$ position similar to that observed in the $\pi^+\pi^-$ channel. The solid line is the result of a fit performed using the same formalism used to fit the $\pi^+\pi^-$ mass spectrum with fixed $S^*/f_0(975)$ parameters but allowing the phase to vary. The experimental resolution has been estimated to have a σ of 25 MeV in the 1.0 GeV region. The fit has a χ^2/NDF of 63/41.

8. STUDY OF THE REACTIONS $(\pi^+/p)p \rightarrow (\pi_f^+/p_f)(\pi^+\pi^-)p_s$ AT 85 GeV/c

Reactions (1) and (2) have been isolated from 2.5×10^6 four-prong events. Momentum balance was obtained by requiring |missing P_x| < 4.0 GeV/c, |missing P_y| < 0.12 GeV/c and |missing P_z| < 0.10 GeV/c. The energy balance was ensured by requiring the Ehrlich mass squared m_X^2 (shown in fig. 24) to be in the region $-0.07 < m_X^2 < 0.15$ GeV^2. Compatibility with Cherenkov information was required for both pions. A comparison between fig. 1(a) and fig. 24 shows enhanced signals from the K^+K^- and $p\bar{p}$ centrally produced final states in the 85 GeV/c data. This is due to a K trigger present only in the 85 GeV/c experiment which suppressed by a factor 2.7 the $\pi^+\pi^-$ channel with respect to the K^+K^- and $p\bar{p}$ channels. The above selection gave 59 953 and 117 802 $\pi^+\pi^-$ events for the π^+ and p beams respectively.

The trigger considerably suppressed beam and target diffraction in the data; the target diffraction was almost completely removed. The residual effects of the beam diffraction in the central x_F dipion region were further reduced through direct removal of resonances. Fig. 25(a) shows the $\pi_f^+\pi^+\pi^-$ effective mass distribution for reaction (1). A broad structure around 1.3 GeV indicates the presence of $a_1(1260)/a_2(1320)$ and the $\pi_2(1670)$ is clearly visible together with higher mass structures. The $\pi_f^+\pi^-$ mass spectrum is shown in fig. 25(b) where strong $\rho(770)$ and $f_2(1270)$ resonances can be seen. These are removed by requiring $m(\pi_f^+\pi^-) > 1.5$ GeV. This cut also removes the $a_1(1260)/a_2(1320)$ and $\pi_2(1670)$ signals in the $\pi_f^+\pi^+\pi^-$ mass distribution. In reaction (2), the forward Δ^{++} (fig. 26(a)) is removed by requiring $m(p_f\pi^+) > 1.33$ GeV while no cut has been applied to the $p_f\pi^-$ mass distribution (fig. 26(b)). After application of these cuts 54% and 57% of the events of the original sample are retained for π^+ and p beams respectively. The resulting Feynman-x_F distribution for the p_s, π_f^+/p_f and the dipion system is shown in fig. 27. The total geometrical acceptance was found to be essentially flat as a function of dipion mass $m(\pi^+\pi^-)$.

The central $\pi^+\pi^-$ mass spectra are shown in fig. 28(a,b) for the π^+ and p beams respectively. For the p data we notice an enhanced $\rho(770)$ signal with respect to the 300 GeV/c data, a drop in the $S^*/f_0(975)$ region and some $f_2(1270)$. The strong $\rho(770)$ signal in these lower energy data indicates that here the contribution coming from I = 1 exchange plays an important role; this effect decreases with energy up to ISR energies where the

$\rho(770)$ signal almost vanishes [14]. The suppression of $\rho(770)$ and $f_2(1270)$ signals in the low t region, already observed in the 300 GeV/c data, is also present in the 85 GeV/c data as can be seen in fig. 29, where the combined π^+ and p data are shown for $t < 0.3$ GeV^2 and $t > 0.3$ GeV^2.

In order to investigate whether the parametrization used to describe the $\pi^+\pi^-$ mass spectrum at 300 GeV/c will also describe the 85 GeV/c data, a fit has been performed to the $\pi^+\pi^-$ mass spectra using the same formalism as described in sect 2. A few modifications have been applied:

(a) The $S^*/f_0(975)$ as well as the X(1470) parameters have been fixed to the values from the 300 GeV/c data, leaving free only the phases which describe the interferences of $S^*/f_0(975)$ and X(1470) with the background.

(b) The $\rho(770)$, which is much larger here than in the 300 GeV/c data, was allowed to interfere with the the $\pi^+\pi^-$ decay mode of the $\omega(783)$ which was parametrized as a Breit–Wigner having 20 MeV full width in order to take account of the experimental resolution ($\pm$ 10 MeV in this mass region). The interference was parametrized as

$$|B_\rho(m) + \alpha B_\omega(m)\epsilon^{i\phi}|^2 \tag{8}$$

The results from the fits are shown in fig. 28 and give a reasonable description of the data (χ^2/NDF=112/86 and 130/86 for π^+ and p beams respectively). We obtain, in expression (8), $\phi = 180 \pm 20^0$ and $\phi = 36 \pm 26^0$ for π^+ and p beams respectively, indicating a negative $\rho - \omega$ interference for the π^+ beam and a positive interference for the p beam. In order to search for $\omega(783)$ production, we have studied the reactions

$$\pi^+ p \rightarrow \pi^+_f(\pi^+\pi^-\pi^0)p_s$$

and

$$pp \rightarrow p_f(\pi^+\pi^-\pi^0)p_s$$

Since, in the 85 GeV/c run, we did not measure γ's, we reconstructed the π^0 as a missing particle. After having removed events belonging to reactions (1) and (2), which balance momentum, events having a missing π^0 have been selected by requiring the missing mass squared to $\pi^+_f/p_f(\pi^+\pi^-)p_s$ to be in the range –0.2 to 0.2 GeV^2. The missing π^0 was then reconstructed by giving it the missing momentum and the π^0 mass. The resulting $\pi^+\pi^-\pi^0$ effective mass distributions for the two reactions are shown in fig. 30, and show the presence of η in both spectra, but a reduced $\omega(783)$ signal in the π^+ incident data with respect to the p incident data.

It is interesting to compare the cross section for production of $\rho(770)$,$S^*/f_0(975)$ and $f_2(1270)$ in the 85 GeV/c p data with the 300 GeV/c experiment. We prefer to give the relative cross sections since, having similar detector and apparatus, systematic errors cancel. We obtain

$$\sigma(\rho(770))_{300}/\sigma(\rho(770))_{85} = 0.44 \pm 0.07 \quad ,$$
$$\sigma(S^*/f_0(975))_{300}/\sigma(S^*/f_0(975))_{85} = 3.12 \pm 1.00 \quad ,$$
$$\sigma(f_2(1270))_{300}/\sigma(f_2(1270))_{85} = 0.83 \pm 0.20 \quad ,$$

Thus, we observe a decrease of the $\rho(770)$ and an increase of the $S^*/f_0(975)$ cross sections as a function of energy.

9. CONCLUSIONS AND COMPARISON WITH OTHER EXPERIMENTS

We have studied the $\pi\pi$ and $K\bar{K}$ systems centrally produced in proton proton collisions at 300 GeV/c and in π^+/p proton collisions at 85 GeV/c. The $\pi^+\pi^-$ effective mass distributions show a $\rho(770)$ signal decreasing as the centre of mass energy increases from $\sqrt{s} = 12.7$ GeV to $\sqrt{s} = 23.8$ GeV. Clear evidence for $S^*/f_0(975)$ production is observed. An analysis performed on the $\pi^+\pi^-$ mass spectrum in the 1.0 GeV region was made using a coupled channel formalism. We found that it was possible to describe the data in the $S^*/f_0(975)$ mass region only if we allowed the $S^*/f_0(975)$ to interfere coherently with the S-wave background. The resulting $S^*/f_0(975)$ parameters were determined to be $m_0 = 979 \pm 4$ MeV, $g_\pi = 0.28 \pm 0.04$, $g_K = 0.56 \pm 0.18$ giving a pole position on sheet II at $(1001 \pm 2) - i(36 \pm 4)$ MeV and a full width of $\Gamma_{S^*/f_0(975)} = 72 \pm 8$ MeV. The value $g_K/g_\pi = 2.0 \pm 0.9$ is in agreement with that found in hadronic J/ψ decay and D_s decay suggesting a substantial $s\bar{s}$ contribution in the $S^*/f_0(975)$ wavefunction. The expected contribution from the $S^*/f_0(975)$ in the $K\bar{K}$ threshold region is easily accomodated in the observed threshold enhancement present in the K^+K^- and $K^0_S K^0_S$ mass spectra obtained in this experiment. Thus, it is possible to describe the $S^*/f_0(975)$ effect with one single resonance.

Evidence is found, in the $\pi^+\pi^-$ spectrum, for a structure with a mass of 1472 ± 12 MeV and a width of 195 ± 33 MeV. This structure may be related to the signal observed in radiative and hadronic J/ψ decay [8,9] and in π induced reactions [10]. If it is a scalar state it may be identified with the $\epsilon/f_0(1400)$.

In order to test if the formalism and $S^*/f_0(975)$ parameters used in the present analysis are also able to describe the data coming from other experiments, we have fitted the $\pi^+\pi^-$ mass spectrum from the ISR experiment [14] and from hadronic J/ψ decay to $\phi\pi^+\pi^-$ [24]. The fits have been performed using the same formalism described in sect. 3 but fixing the $S^*/f_0(975)$ and X(1470) parameters while the interference phases, as well as the resonance amplitudes, have been allowed to vary. The results from the fits are shown in fig. 31(a,b) for ISR and Mark III data respectively and show good agreement with the data.

A study has been performed of the four-momentum transfer behaviour of the $\rho(770)$, $S^*/f_0(975)$, $\phi(1020)$, $f_2(1270)$, $f_2'(1525)$ and $\theta/f_2(1720)$. We observe that $S^*/f_0(975)$ and $\theta/f_2(1720)$ are produced more at low t relative to the $\rho(770)$, $\phi(1020)$, $f_2(1270)$ and $f_2'(1525)$. We find a decrease of the $\rho(770)$ and an increase of the $S^*/f_0(975)$ cross sections as a function of energy in the Feynman-x_F range covered by these experiments.

ACKNOWLEDGMENTS

We acknowledge N. Isgur, A.B. Kaidalov and M. Pennington for useful discussions.

REFERENCES

[1] D.L. Scharre et al., Phys Lett. 97B (1980) 329;

C. Edwards et al., Phys. Rev. Lett. 49 (1982) 259.

[2] C. Edwards et al., Phys. Rev. Lett. 48 (1982) 458;

[3] R.M. Baltrusaitis et al., Phys. Rev. D35 (1987) 2077;

[4] J.E. Augustin et al., Phys. Rev. Lett. 60 (1988) 2238.

[5] T.A. Armstrong et al., Phys. Lett. 227B (1989) 186.

[6] S. Sharpe, proc. of the BNL Workshop on Glueballs, Hybrids and Exotic Hadrons, ed. S.U. Chung, Upton, New York (1988), (AIP, New York).

[7] J. Adler et al., proc. of the XXIV Int. Conf. on High-Energy Physics, Munich, R. Kotthaus and J.H. Kühn eds., Springer-Verlag, Munich (1989).

[8] L. Köpke and N. Wermes, Phys. Rep. 174 (1989) 67.

[9] A. Falvard et al., Phys. Rev. D38 (1988) 2706.

[10] B. Hyams et al., Nucl. Phys. B64 (1973) 134;

S. Protopopescu et al., Phys. Rev. D7 (1973) 1280.

[11] H. Marsiske et al., Phys. Rev. D41 (1990) 3324.

[12] J.C. Anjos et al., Phys. Rev. Lett. 62 (1989) 125.

[13] K.L. Au et al., Phys. Rev. D35 (1987) 1633.

[14] T. Akesson et al., Nucl. Phys. B264 (1986) 154.

[15] R. Jaffe, Phys. Rev. D15 (1977) 267.

[16] J. Weinstein and N. Isgur, Phys. Rev. D41 (1990) 2236.

[17] T.A. Armstrong et al., Phys. Lett. 146B (1984) 273.

[18] T.A. Armstrong et al., Nucl. Instr. and Meth. A274 (1989) 165.

[19] R. Ehrlich et al., Phys. Rev. Lett. 20 (1968) 686.

[20] S.M. Flatté et al., Phys. Lett. 38B (1972) 232.

[21] Review of Particles Properties, Phys. Lett. B239 (1990).

[22] A. Breakstone at al., Zeitschrift für Phys. C31 (1986) 185.

[23] K.F. Liu et al., Phys. Rev. D40 (1989) 3648.

[24] B. Lockman, proc. of the 3^{rd} Int. Conf. on Hadron Spectroscopy, Ajaccio, ed. Frontiéres (1989).

Table I

Fit parameters of the $\pi^+\pi^-$ spectrum at 300 GeV/c.

α	0.813
β	5.528
γ	-0.764
A_ρ	0.0314
A_f	0.0971
A_θ	0.216
A_s	0.195
A_X	0.0247
δ_1	23°
δ_2	159°
m_X	1472 MeV
Γ_X	195 MeV
m_0	979 MeV
g_π	0.28
g_K	0.56
Pole sheet II	1001 - 36i MeV
Pole sheet III	912 - 94i MeV

FIGURE CAPTIONS

Fig. 1 (a) Ehrlich mass squared distribution for candidates to the reaction $pp \rightarrow p_f(\pi^+\pi^-)p_s$ at 300 GeV/c.

(b) Ehrlich mass squared distribution for events having one particle identified as K, p or ambiguous K/p by the Cherenkov information.

Fig. 2 $p\pi$ effective mass distributions at 300 GeV/c:

(a) $m(p_f\pi^+)$; (b) $m(p_f\pi^-)$; (c) $m(p_s\pi^+)$; (d) $m(p_s\pi^-)$.

Fig. 3 $\pi^+\pi^-$ effective mass distribution at 300 GeV/c.

Fig. 4 Feynman-x_F distribution for the slow proton, the dipion system and the fast proton at 300 GeV/c.

Fig. 5 $\pi^+\pi^-\pi^0$ effective mass spectrum for 4-prong events having two γ's coming from a π^0 reconstructed in the electromagnetic calorimeter at 300 GeV/c.

Fig. 6 (a) Expanded view of the fit to the $\pi^+\pi^-$ spectrum in the 1.5 GeV region at 300 GeV/c. The fit has been performed without including a Breit–Wigner in the 1.5 GeV region.

(b) As in (a) but with a new Breit–Wigner term to describe the 1.5 GeV region and a $\theta/f_2(1720)$ contribution included in the fit.

Fig. 7 (a) $\pi^+\pi^-$ effective mass distribution at 300 GeV/c. The line is the result from the fit described in the text.

(b) As in (a) but on a logarithmic scale.

Fig. 8 (a) K^+K^- effective mass spectrum at 300 GeV/c. The dashed histogram represents the estimated contamination from the $\pi^+\pi^-$ channel.

(b) K^+K^- effective mass spectrum with the $\pi^+\pi^-$ contamination subtracted. The band drawn in the threshold region represents the estimated contribution from the $S^*/f_0(975)$ measured in the $\pi^+\pi^-$ spectrum with one-standard deviation.

Fig. 9 (a) Geometrical acceptance for the $\pi^+\pi^-$ system as a function of the $\pi^+\pi^-$ effective mass at 300 GeV/c.

(b) Geometrical acceptance for the K^+K^- system as a function of the K^+K^- effective mass.

Fig. 10 (a) Ehrlich mass squared distribution, at 300 GeV/c, for candidates to the K^+K^- final state after having removed only events having identified pions.

(b) K^+K^- effective mass distribution, for the Ehrlich mass squared shown in (a), in the threshold region.

FIGURE CAPTIONS (Cont'd)

Fig. 11 (a) $\pi^+\pi^-$ effective mass at the V^0 vertex for events candidates to the $K^0_S K^0_S$ channel for the 300 GeV/c data.

(b) Geometrical acceptance for the $K^0_S K^0_S$ system.

Fig. 12 $K^0_S K^0_S$ effective mass distribution obtained by combining the 85 GeV/c and the 300 GeV/c data. The curve represents the $S^*/f_0(975)$ contribution from the fit to the $\pi^+\pi^-$ data.

Fig. 13 (a) Double exchange graph.

(b) Four-momentum transfer distribution at the upper vertex, $|t_1|$.

(c) Four-momentum transfer distribution at the lower vertex, $|t_2|$.

(d) $t = |t_1 + t_2|$.

Fig. 14 (a) $\pi^+\pi^-$ effective mass for $t < 0.3$ GeV^2 and (b) $\pi^+\pi^-$ effective mass for $t > 0.3$ GeV^2. The data are from the 300 GeV/c run.

Fig. 15 $\pi^+\pi^-$ effective mass distributions in different t intervals at 300 GeV/c.

Fig. 16 (a) Phases distributions as functions of t; δ_1: open points, δ_2: black points.

(b) Geometrical acceptance as a function of t.

Fig. 17 (1/t) dN/dt distributions for: (a) $S^*/f_0(975)$, (b) $f_2(1270)$, (c) $\rho(770)$ and (d) X(1470). Open points: uncorrected data; black points: data corrected for geometrical acceptance.

Fig. 18 (a) K^+K^- effective mass distribution for $t < 0.3$ GeV^2 and (b) K^+K^- effective mass for $t > 0.3$ GeV^2. The data are from the 300 GeV/c run.

Fig. 19 (1/t) dN/dt distributions for: (a) $f_2'(1525)$, (b) $\theta/f_2(1720)$. Open points: uncorrected data; black points: corrected data.

Fig. 20 K^+K^- effective mass distribution for: (a) $t < 0.3$ GeV^2 and (b) $t > 0.3$ GeV^2 at 300 GeV/c after having removed only events having identified pions. (c) (1/t) dN/dt distribution for $\phi(1020)$. Open points: uncorrected data; black points: corrected data.

Fig. 21 m($\gamma_1\gamma_2$) vs m($\gamma_3\gamma_4$) lego plot for events having 4 γ reconstructed in the electromagnetic calorimeter which balance momentum. The data are from the 300 GeV/c run.

Fig. 22 (a) $\gamma\gamma$ effective mass distribution for four-γ events after having required the other combination to be in the π^0 region. (b) $p_f\pi^0$ effective mass distribution. The data are from the 300 GeV/c run.

FIGURE CAPTIONS (Cont'd)

Fig. 23 $\pi^0\pi^0$ effective mass distribution at 300 GeV/c. The curve is the result from the fit described in the text.

Fig. 24 Ehrlich mass distribution for the 85 GeV/c data.

Fig. 25 (a) $\pi_f^+\pi^+\pi^-$ effective mass distribution for π^+ beam data at 85 GeV/c.

(b) $\pi_f^+\pi^-$ effective mass for π^+ beam.

Fig. 26 (a) $p_f\pi^+$ effective mass for p beam data at 85 GeV/c.

(b) $p_f\pi^-$ effective mass.

Fig. 27 Feynman-x_F distribution for the slow proton, the dipion system and the fast proton for the 85 GeV/c data.

Fig. 28 $\pi^+\pi^-$ effective mass distributions for: (a) π^+ beam and (b) p beam at 85 GeV/c. The curves are the results from the fits described in the text.

Fig. 29 $\pi^+\pi^-$ effective mass distributions summed over π^+ and p beams at 85 GeV/c for: (a) $t < 0.3$ GeV^2 and (b) $t > 0.3$ GeV^2.

Fig. 30 $\pi^+\pi^-\pi^0$ effective mass distributions for: (a) π^+ beam and (b) p beam at 85 GeV/c.

Fig. 31 (a) $\pi^+\pi^-$ effective mass distribution from ISR [13,14]. The curve is the result from the fit described in the text.

(b) $\pi^+\pi^-$ effective mass from hadronic J/ψ decay to $\phi\pi^+\pi^-$ [24]. The curve is the result from the fit described in the text.

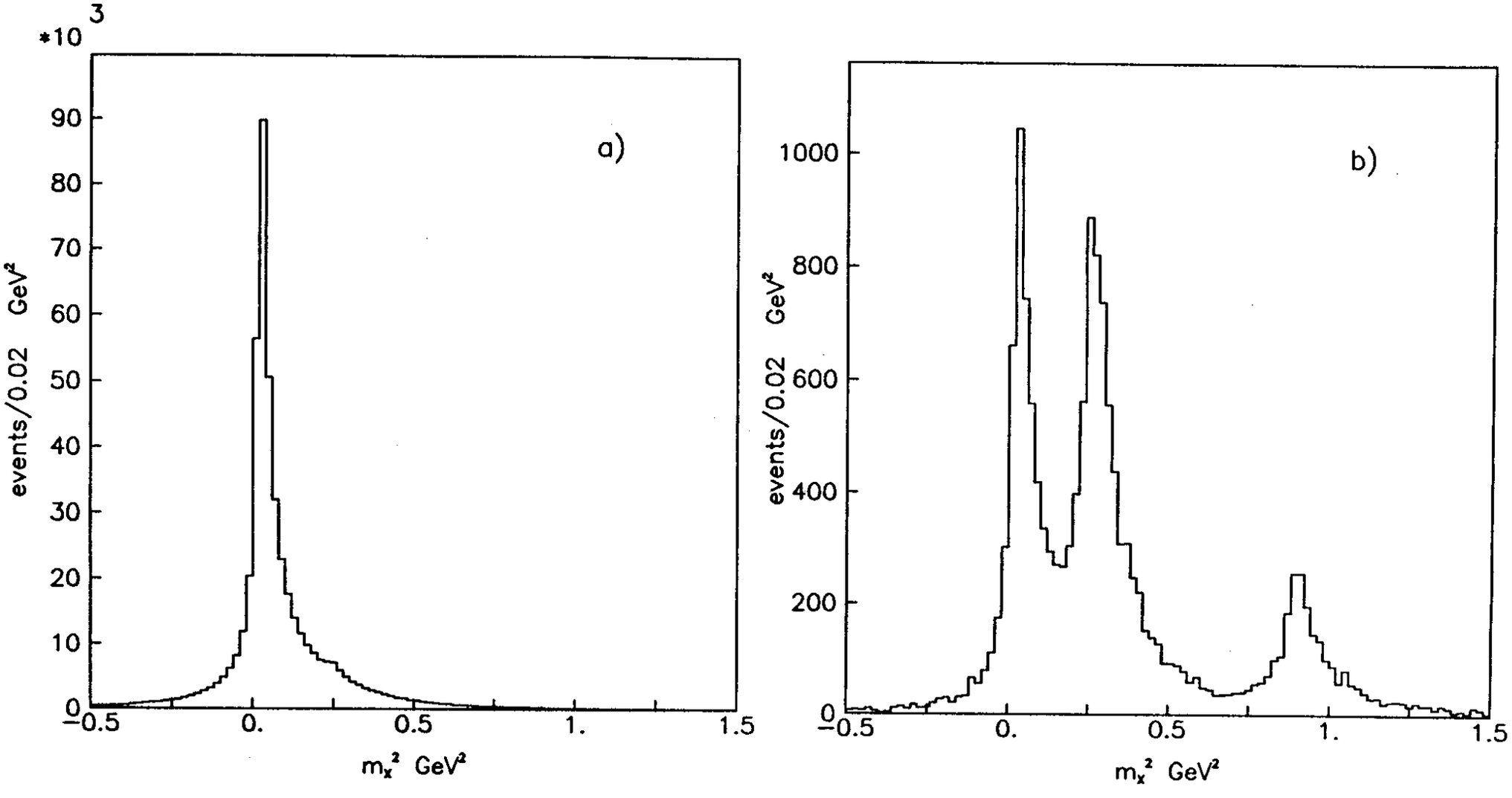
*10 3
90
80
70
60
50
40
30
20
10
0
events/0.02 GeV²
a)
−0.5
0.
0.5
1.
1.5
m_x² GeV²
1000
800
600
400
200
0
events/0.02 GeV²
b)
−0.5
0.
0.5
1.
1.5
m_x² GeV²

Fig. 1

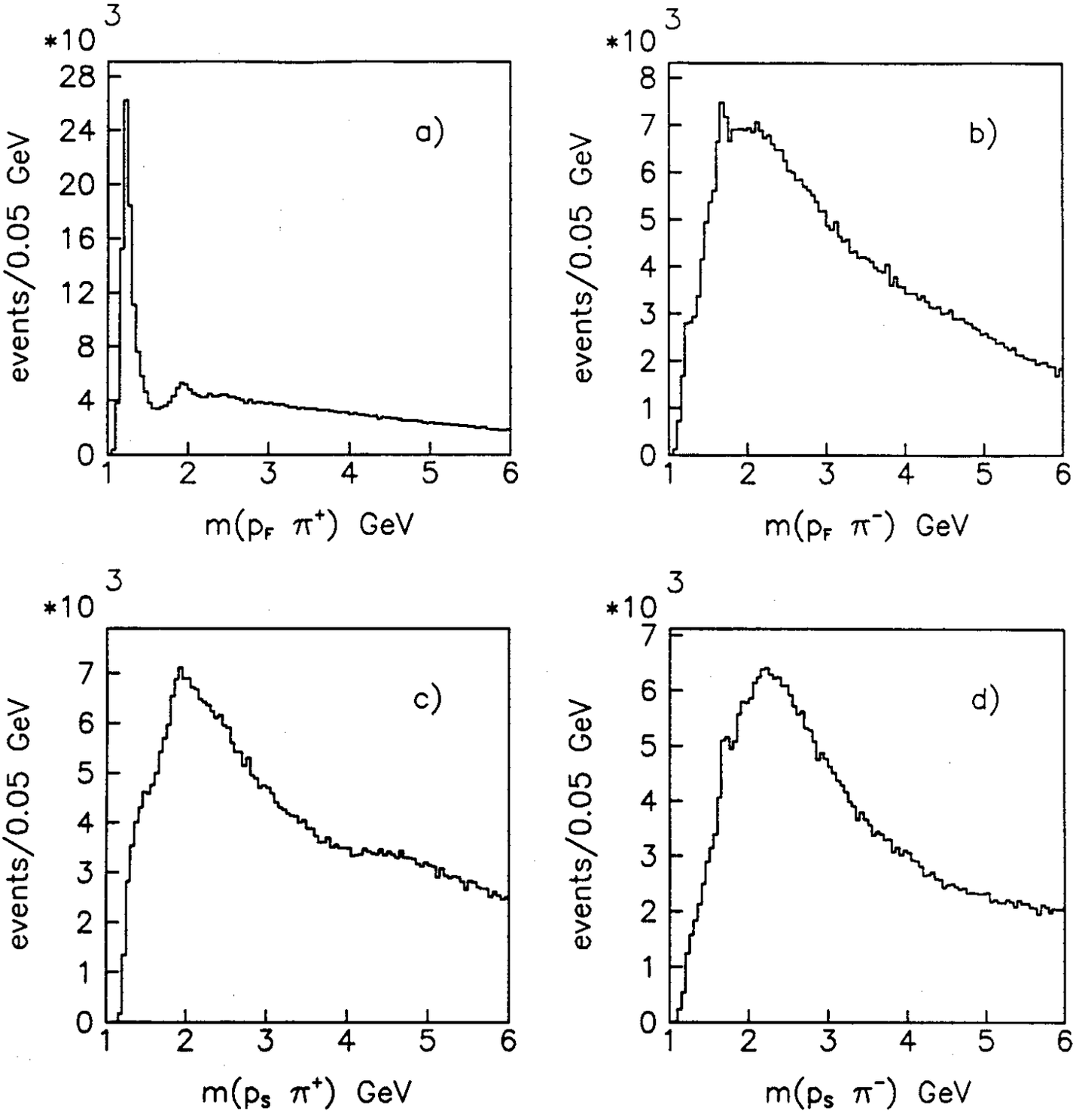

Fig. 2

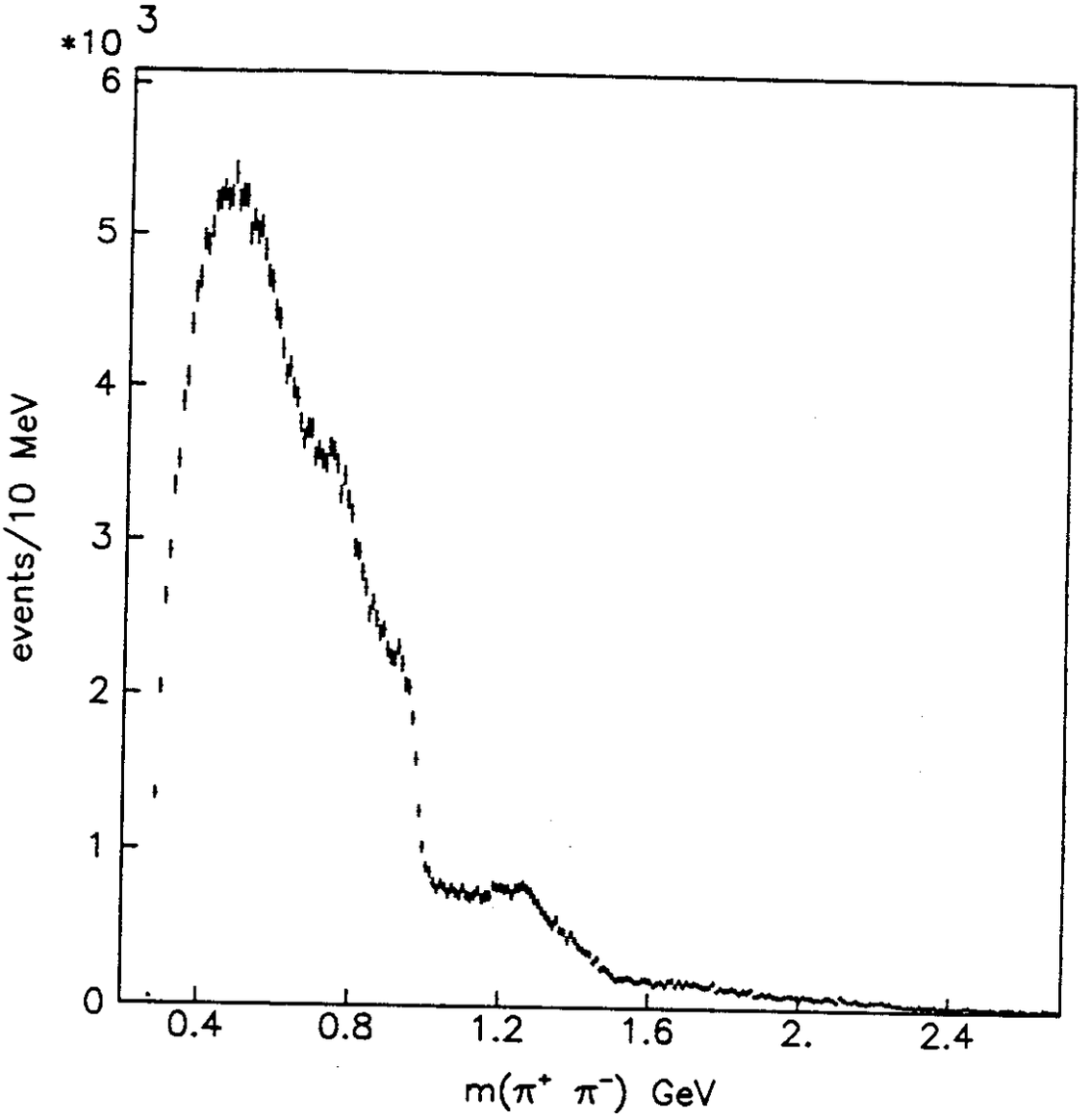

Fig. 3

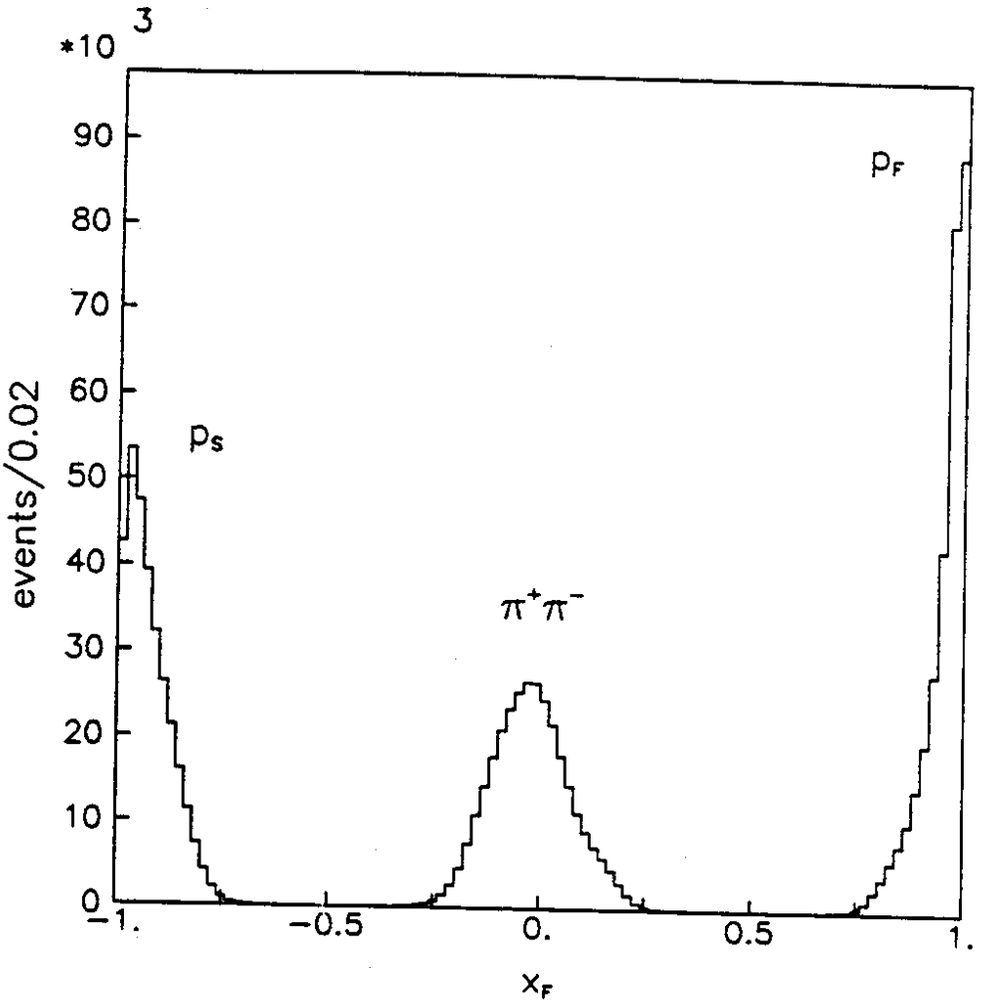

Fig. 4

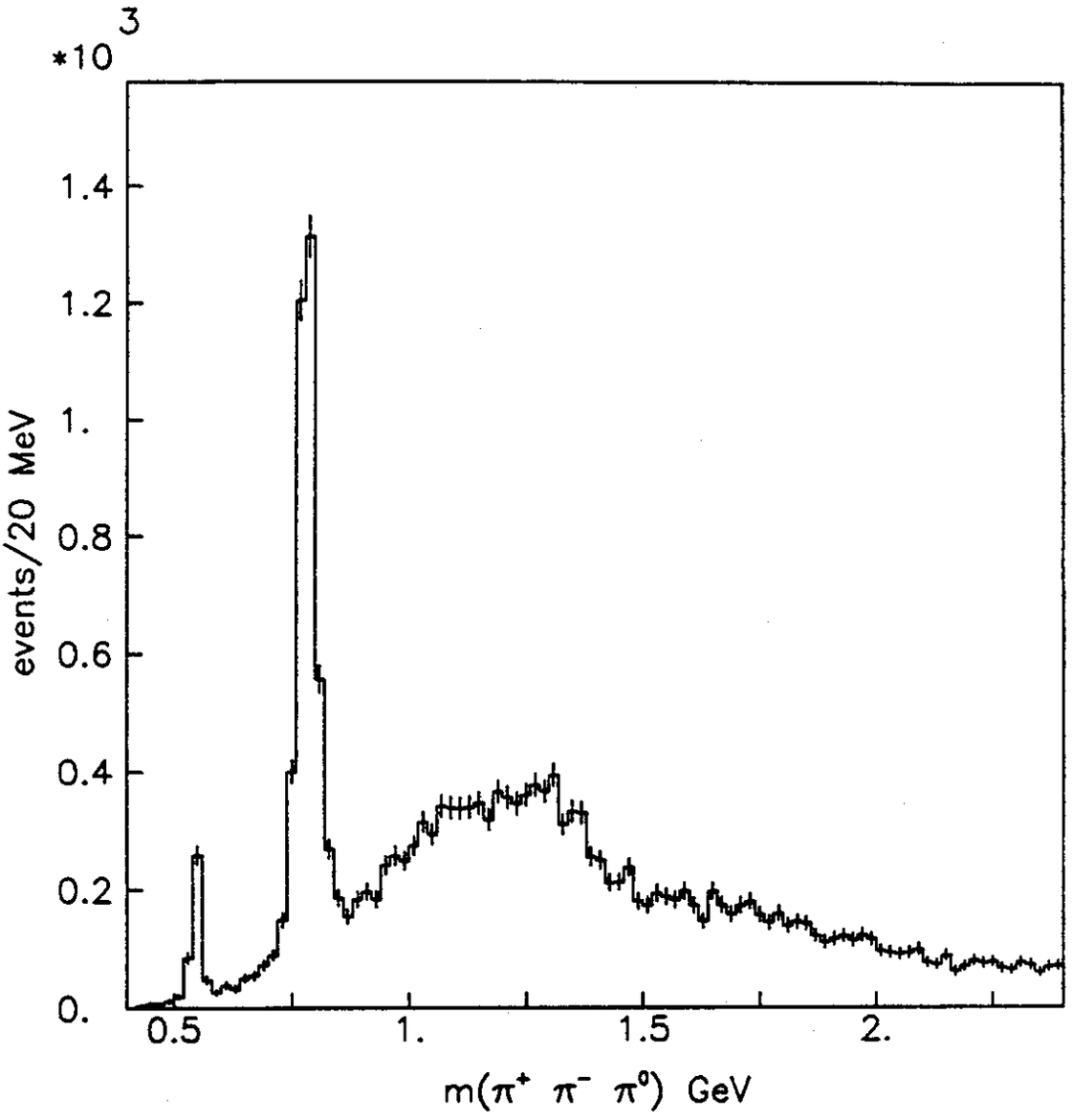

Fig. 5

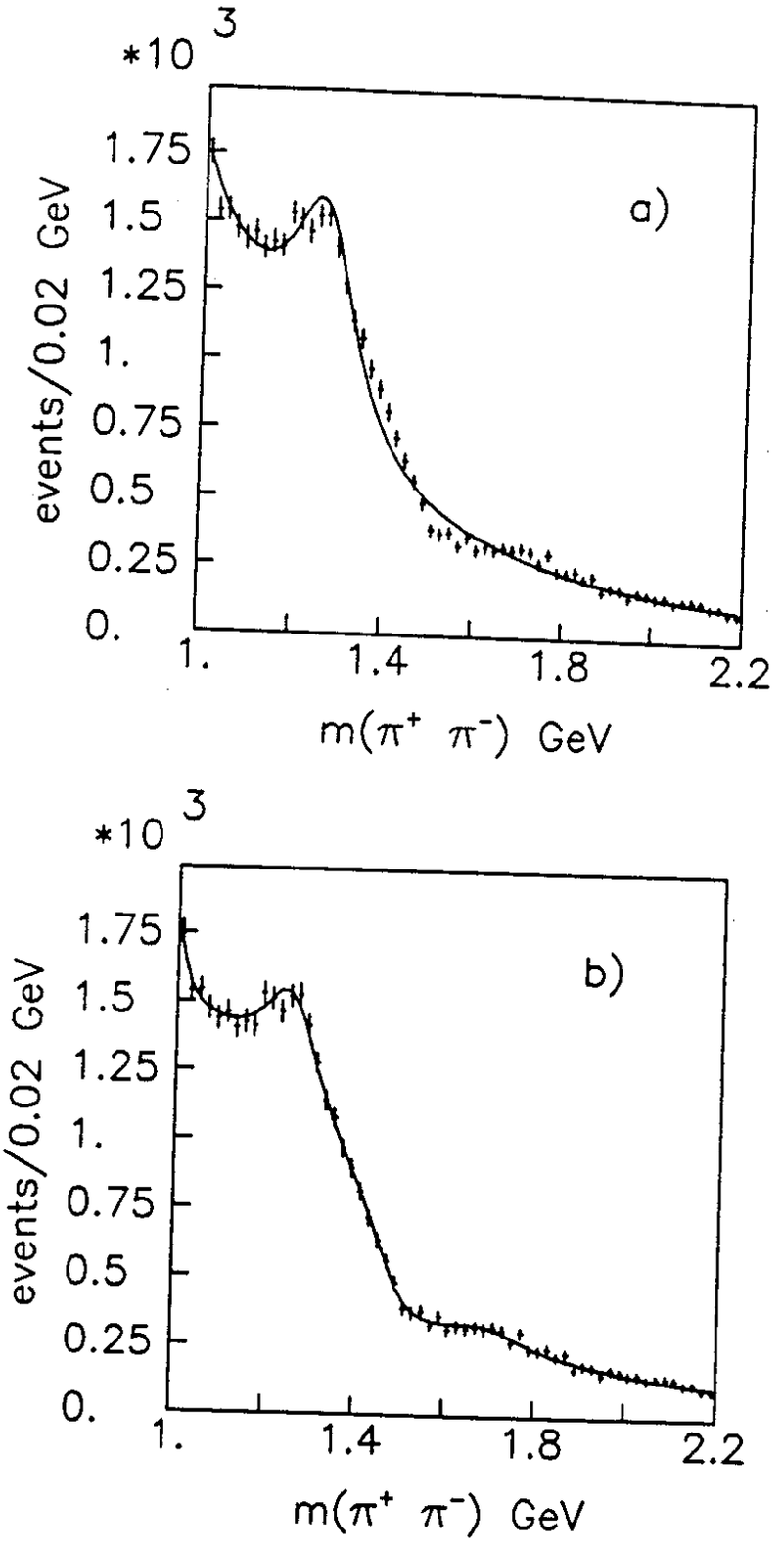
*10 3
1.75
1.5
1.25
1.
0.75
0.5
0.25
0.
events/0.02 GeV
a)
1.
1.4
1.8
2.2
m(π+ π−) GeV
*10 3
1.75
1.5
1.25
1.
0.75
0.5
0.25
0.
events/0.02 GeV
b)
1.
1.4
1.8
2.2
m(π+ π−) GeV

Fig. 6

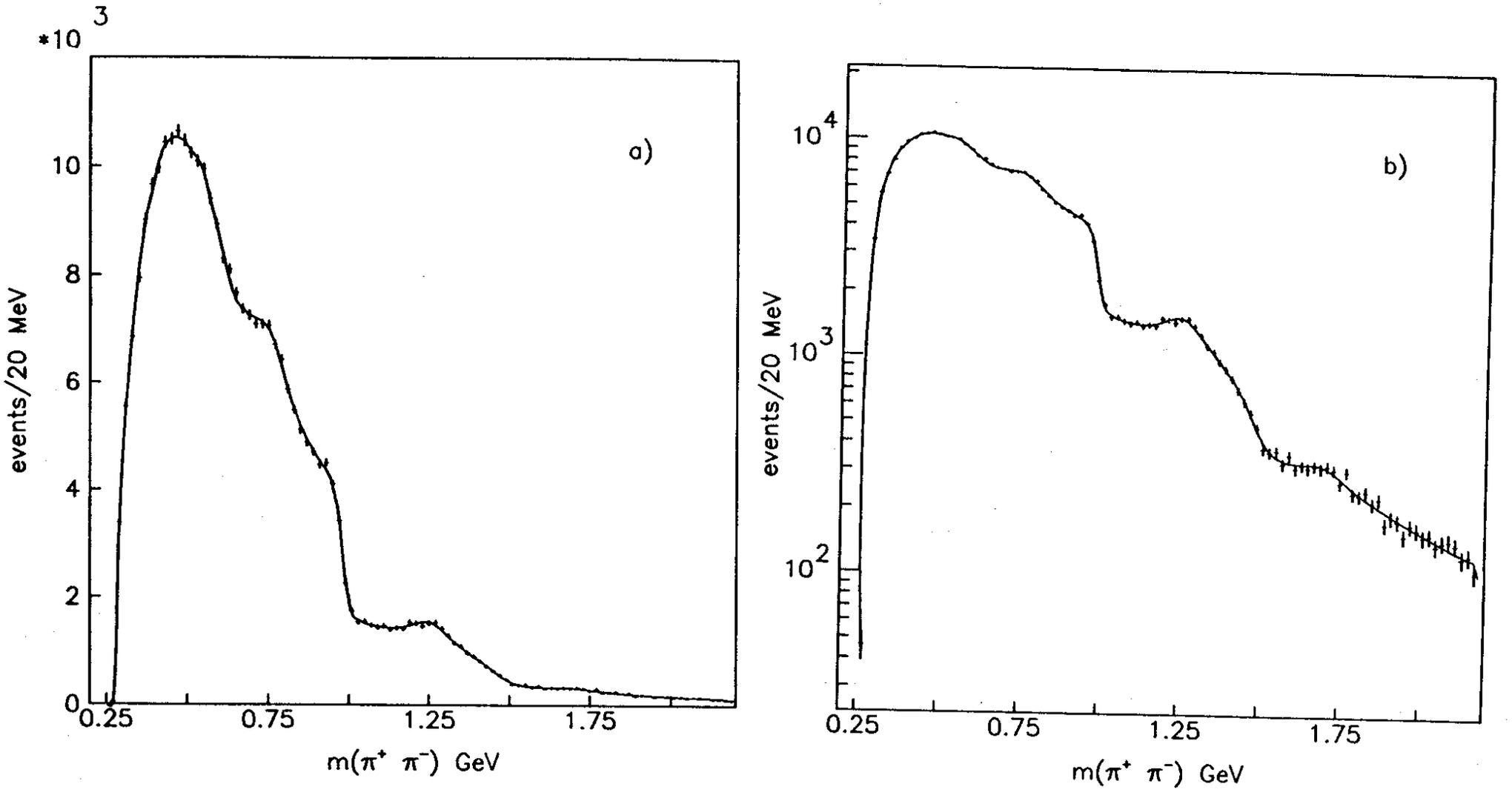

Fig. 7

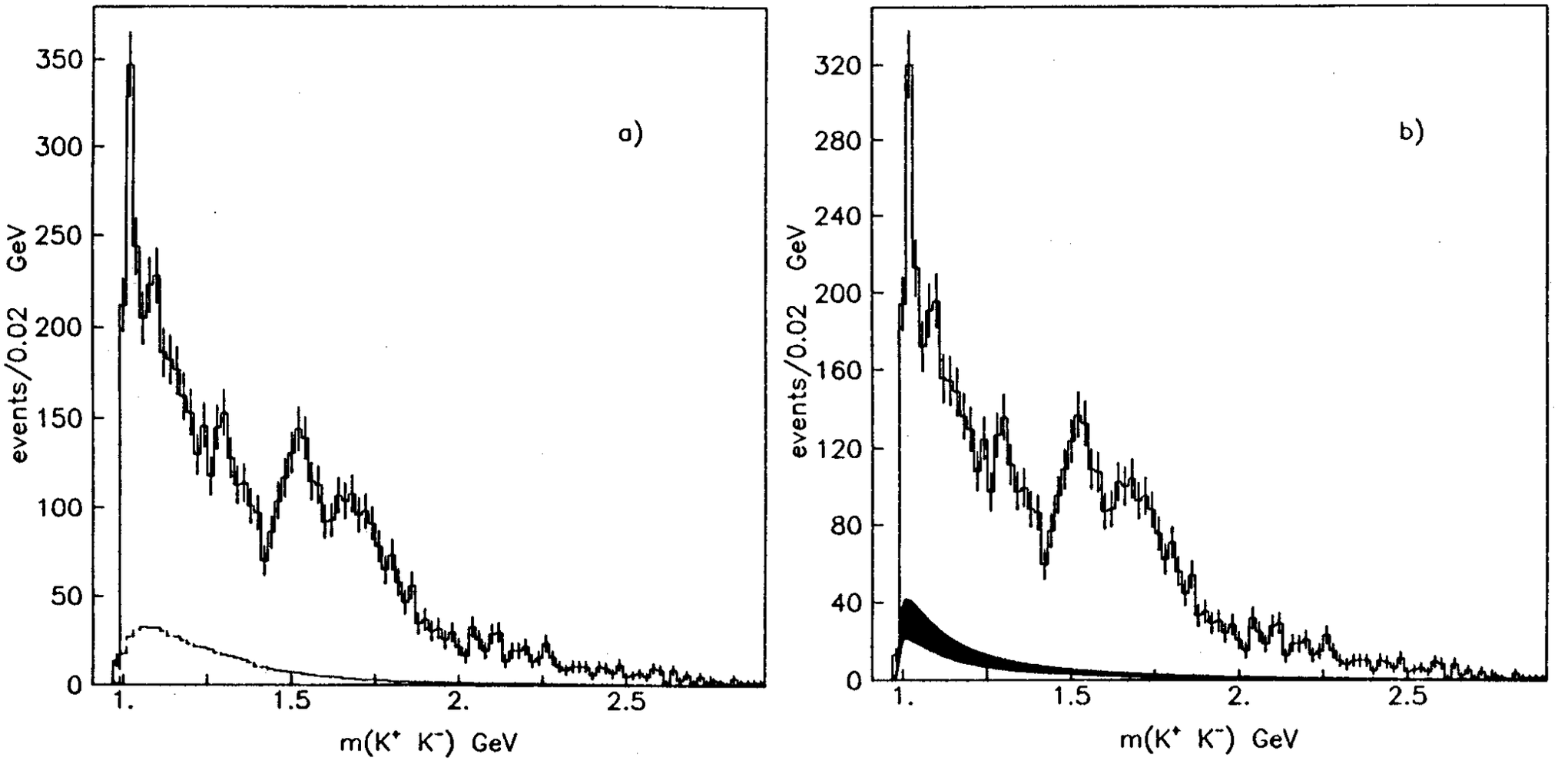
a)
b)
events/0.02 GeV
m(K⁺ K⁻) GeV
0
50
100
150
200
250
300
350
40
80
120
160
200
240
280
320
1.
1.5
2.
2.5

Fig. 8

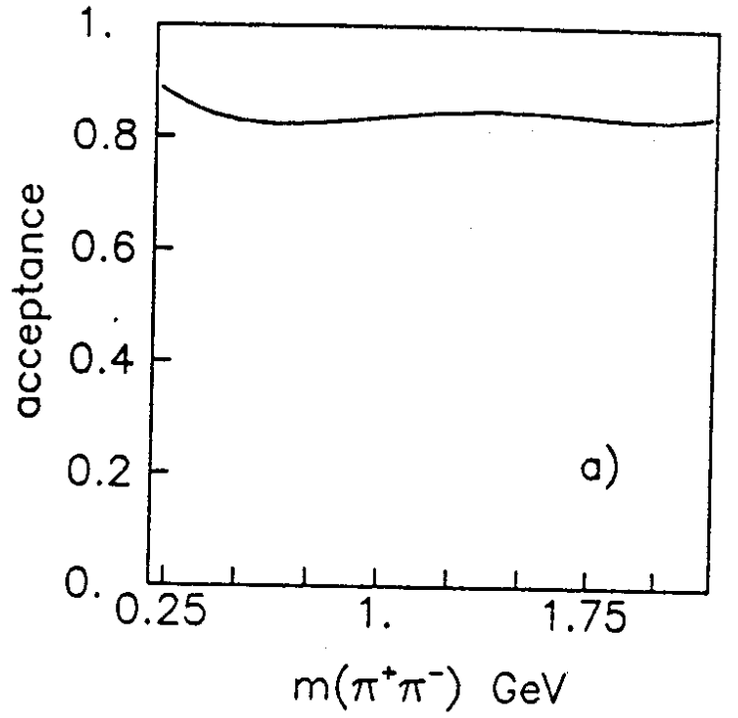
1.
0.8
0.6
0.4
0.2
0.
acceptance
a)
0.25
1.
1.75
m(π⁺π⁻) GeV

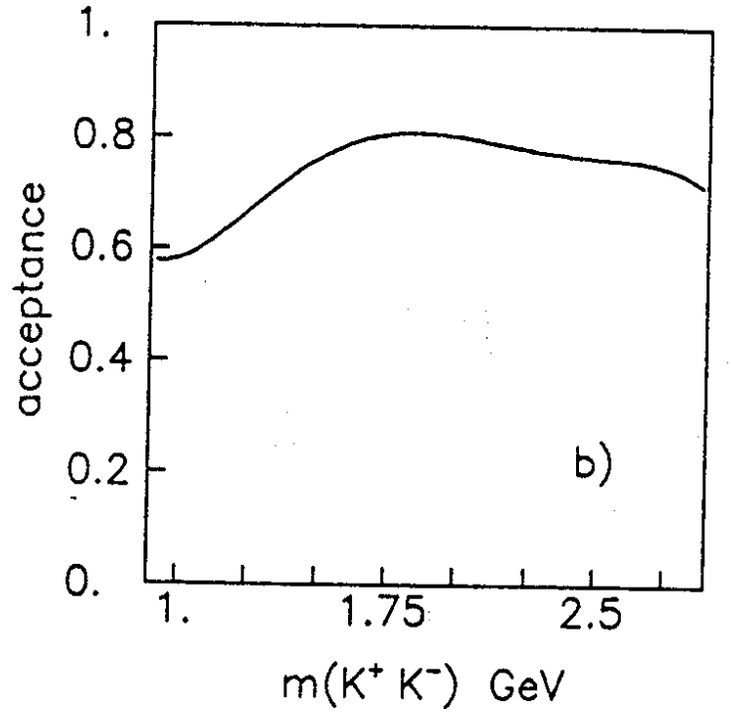
1.
0.8
0.6
0.4
0.2
0.
acceptance
b)
1.
1.75
2.5
m(K⁺ K⁻) GeV

Fig. 9

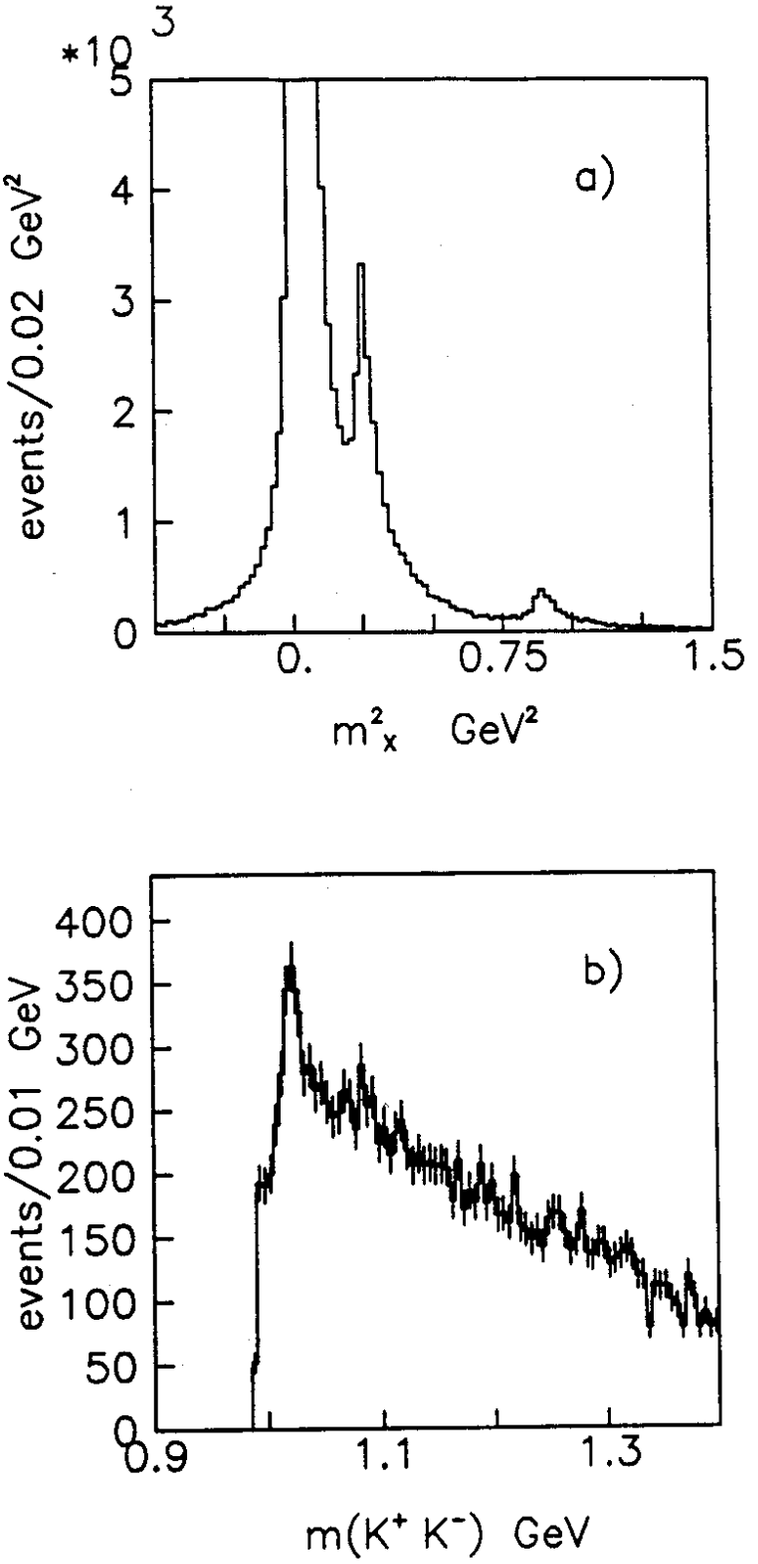
*10 3
5
4
3
2
1
0
events/0.02 GeV²
a)
0.
0.75
1.5
m²x GeV²
400
350
300
250
200
150
100
50
0
events/0.01 GeV
b)
0.9
1.1
1.3
m(K⁺ K⁻) GeV

Fig. 10

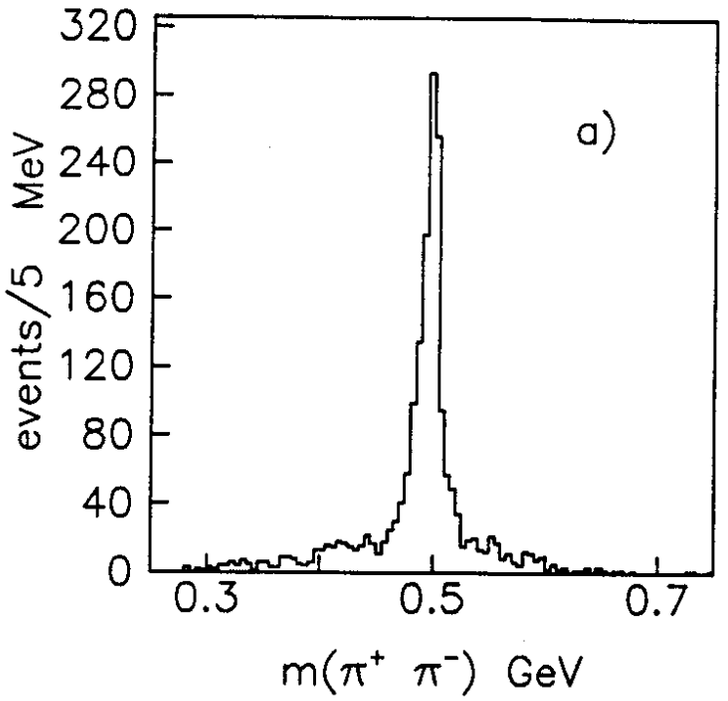
320
280
240
200
160
120
80
40
0
events/5 MeV
a)
0.3
0.5
0.7
m(π+ π−) GeV

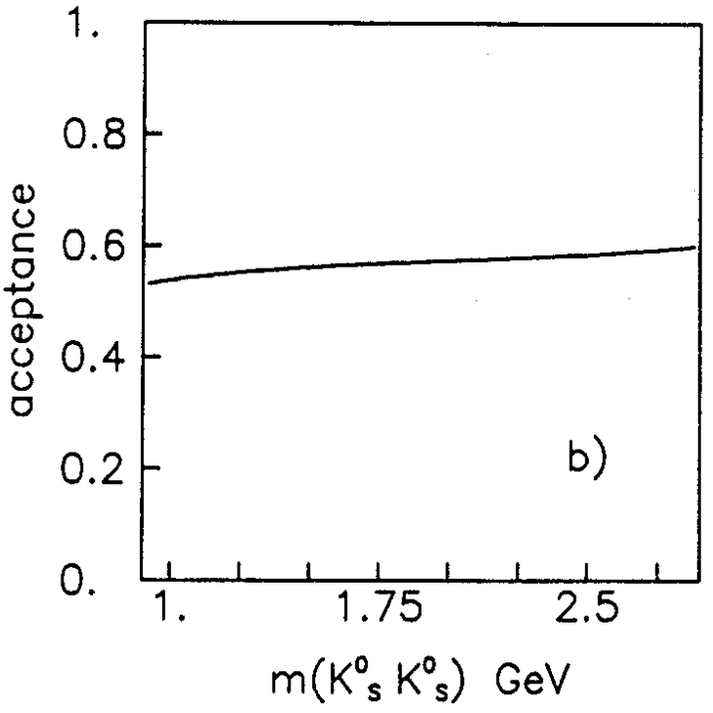
1.
0.8
0.6
0.4
0.2
0.
acceptance
b)
1.
1.75
2.5
m(K°s K°s) GeV

Fig. 11

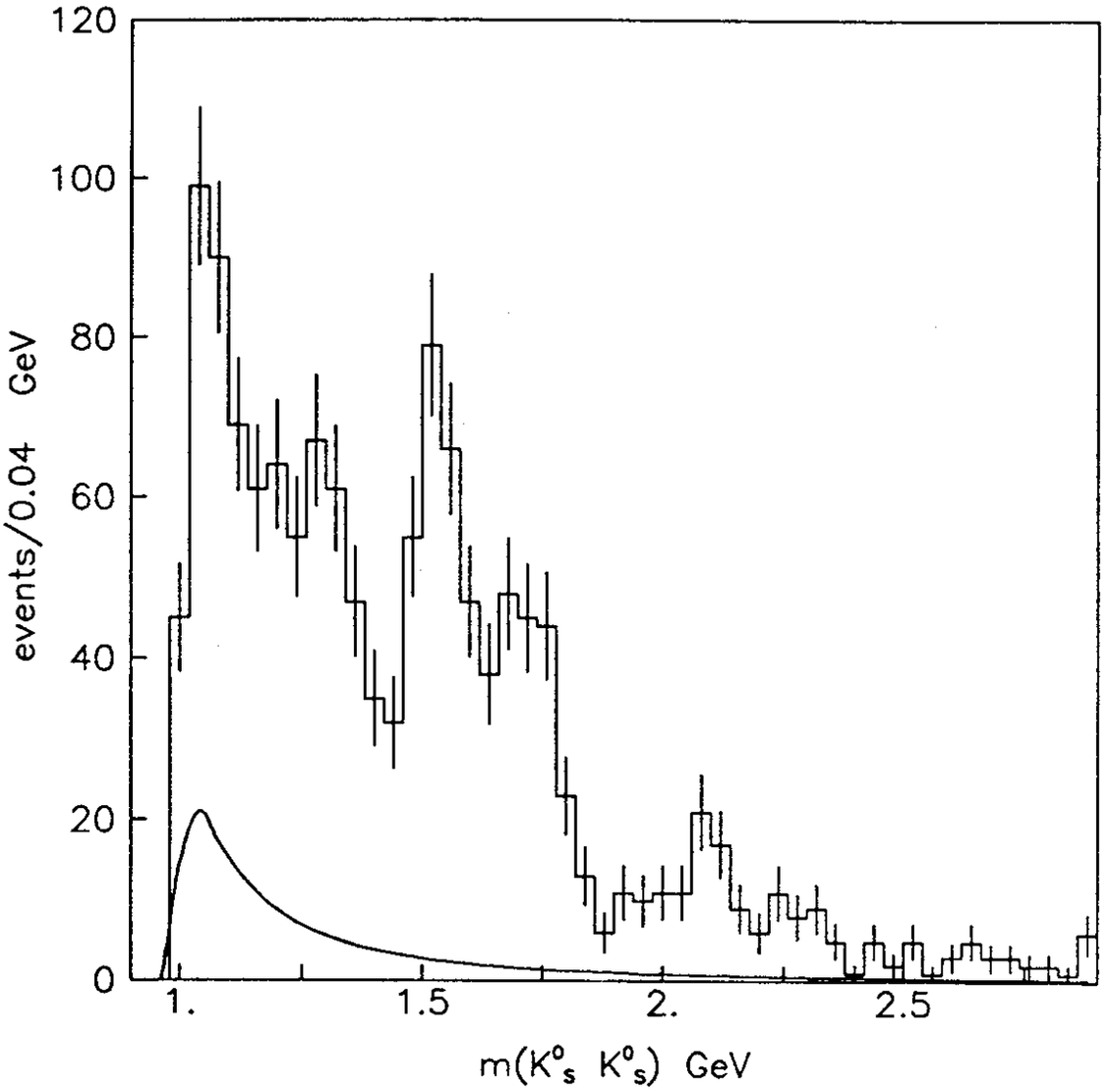

Fig. 12

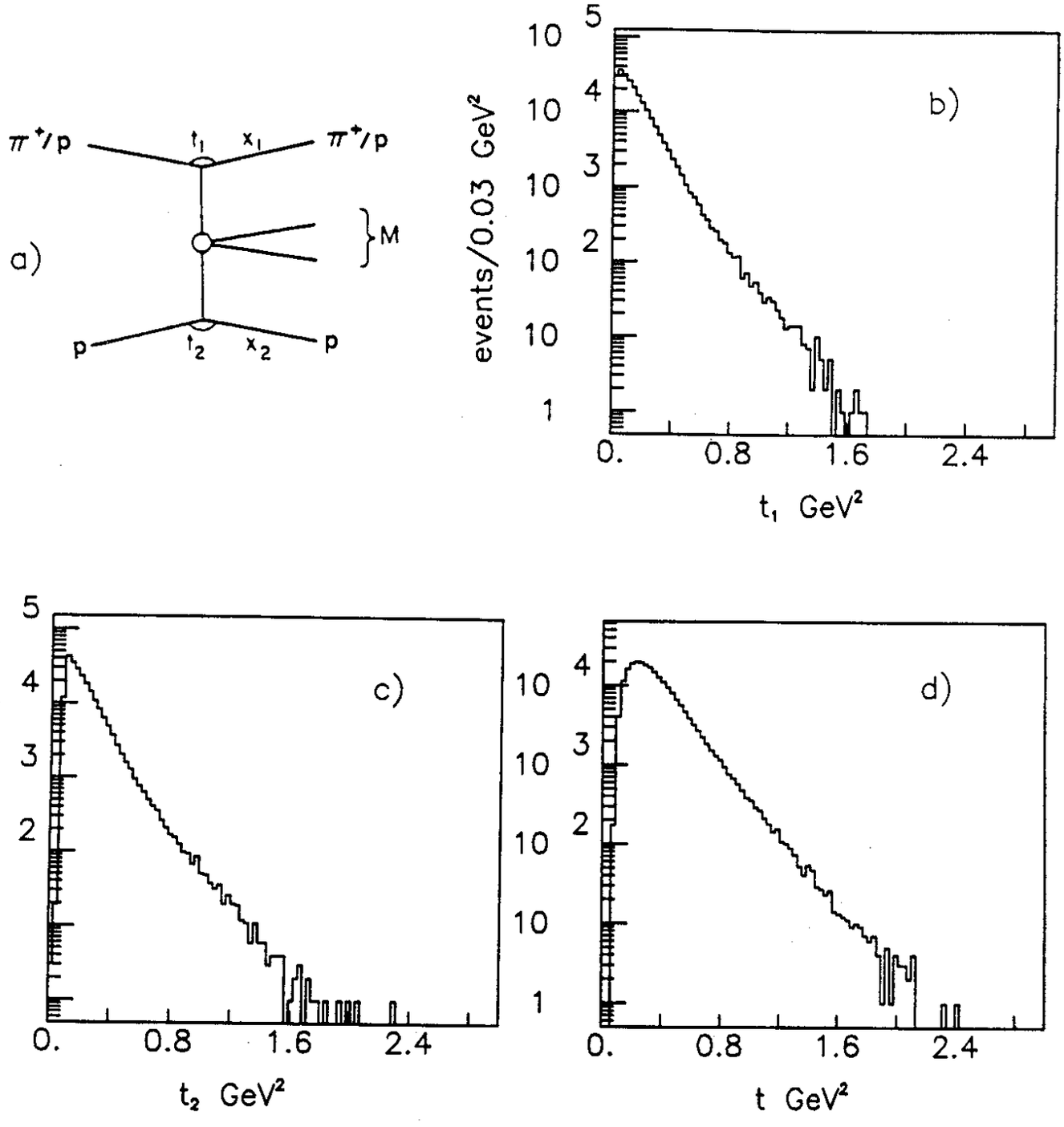
a)
π^+/p
t_1
x_1
π^+/p
M
p
t_2
x_2
p
b)
events/0.03 GeV²
t_1 GeV²
c)
events/0.03 GeV²
t_2 GeV²
d)
t GeV²
0.
0.8
1.6
2.4

Fig. 13

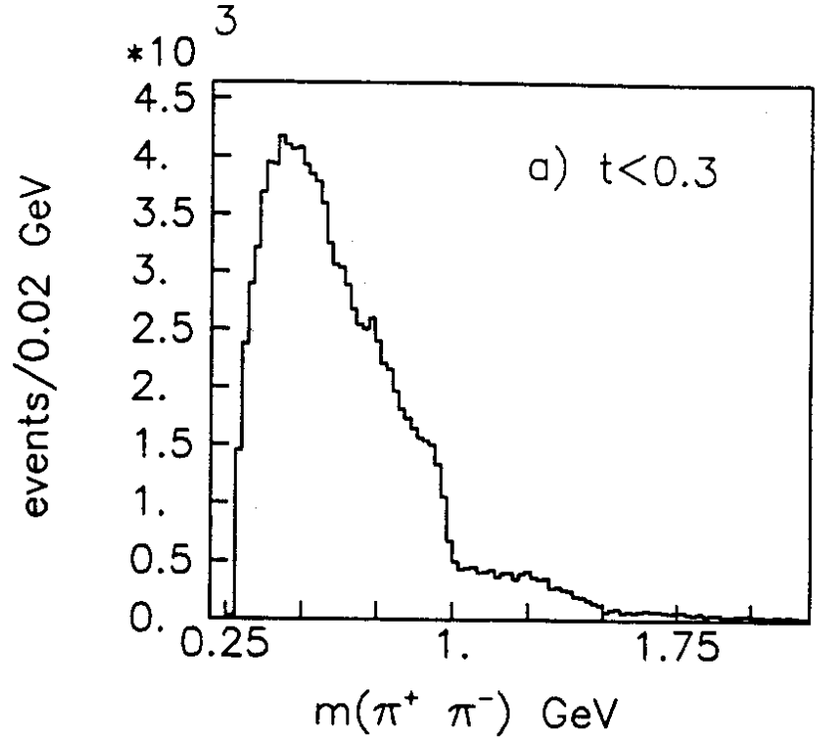
*10 3
4.5
4.
3.5
3.
2.5
2.
1.5
1.
0.5
0.
events/0.02 GeV
a) t<0.3
0.25
1.
1.75
m(π+ π−) GeV

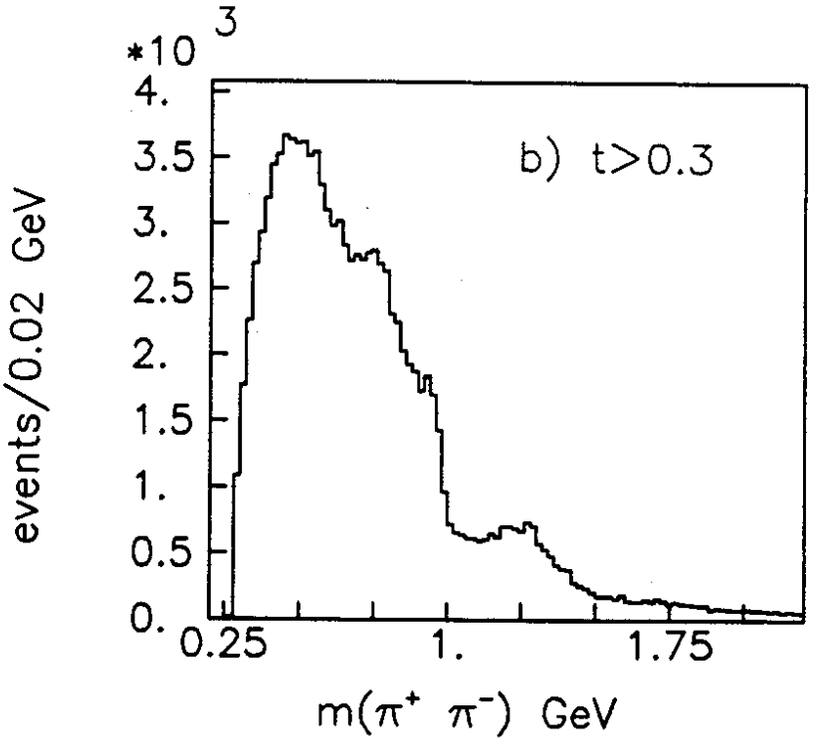
*10 3
4.
3.5
3.
2.5
2.
1.5
1.
0.5
0.
events/0.02 GeV
b) t>0.3
0.25
1.
1.75
m(π+ π−) GeV

Fig. 14

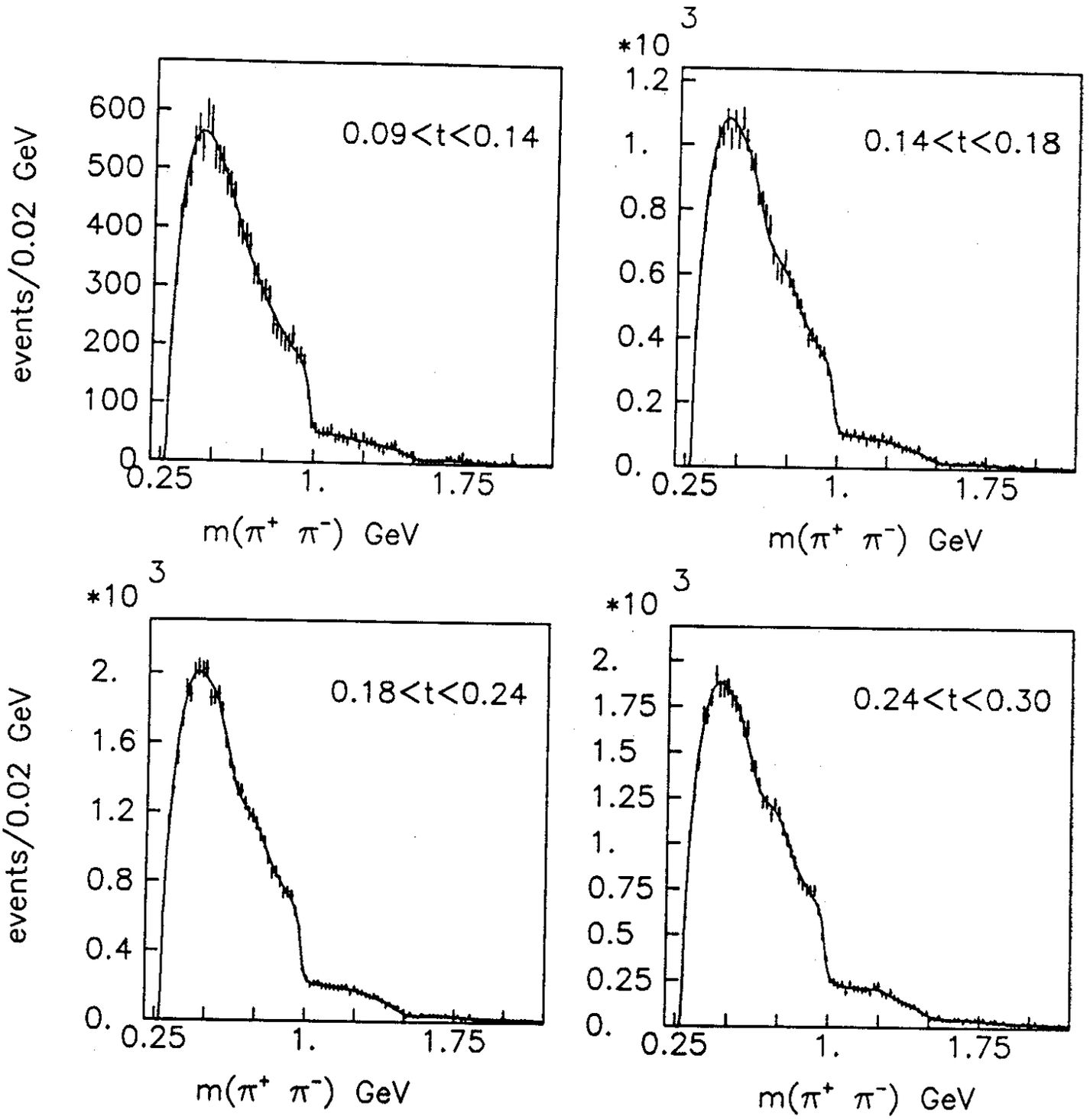
events/0.02 GeV
0.09<t<0.14
0.14<t<0.18
0.18<t<0.24
0.24<t<0.30
*10 3
m(π+ π−) GeV
0.25
1.
1.75

Fig. 15

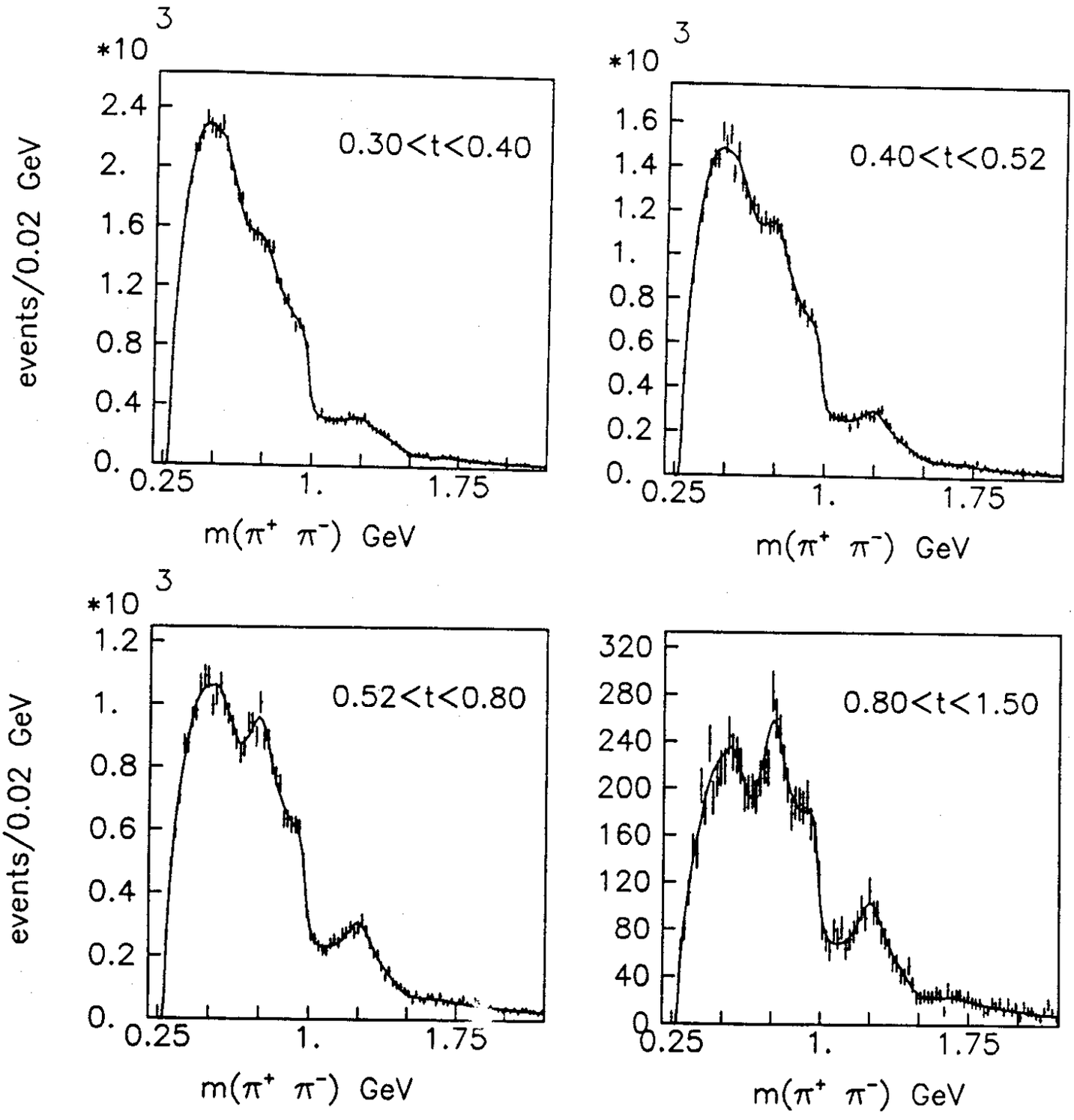
*10 3
events/0.02 GeV
0.30<t<0.40
0.40<t<0.52
0.52<t<0.80
0.80<t<1.50
m(π+ π−) GeV
0.25
1.
1.75

Fig. 15 (cont)

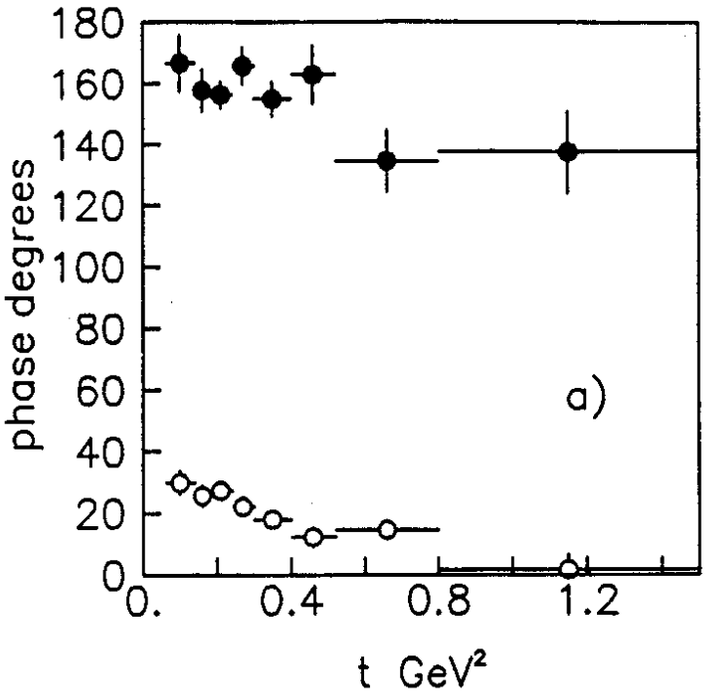
180
160
140
120
100
80
60
40
20
0
phase degrees
0.
0.4
0.8
1.2
t GeV²
a)

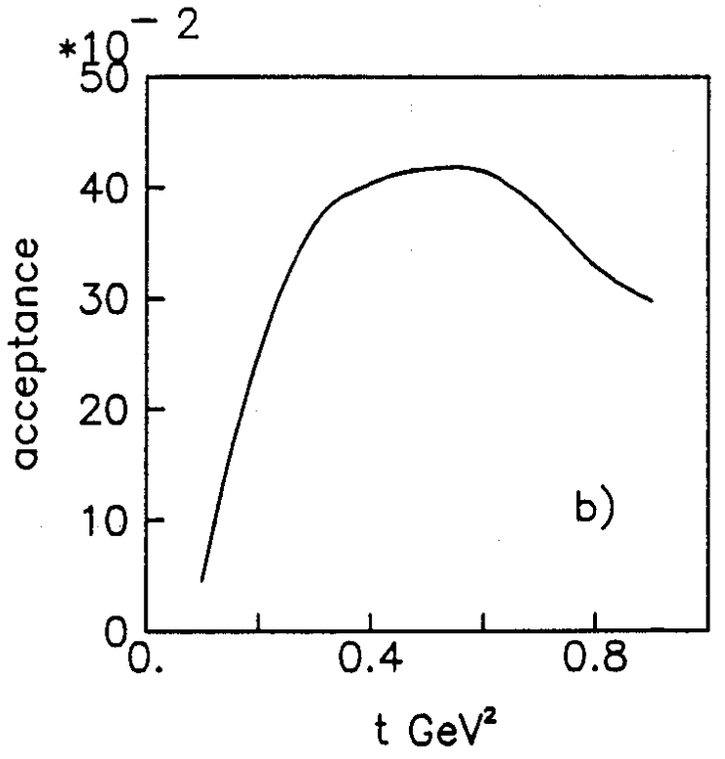
*10⁻ 2
50
40
30
20
10
0
acceptance
0.
0.4
0.8
t GeV²
b)

Fig. 16

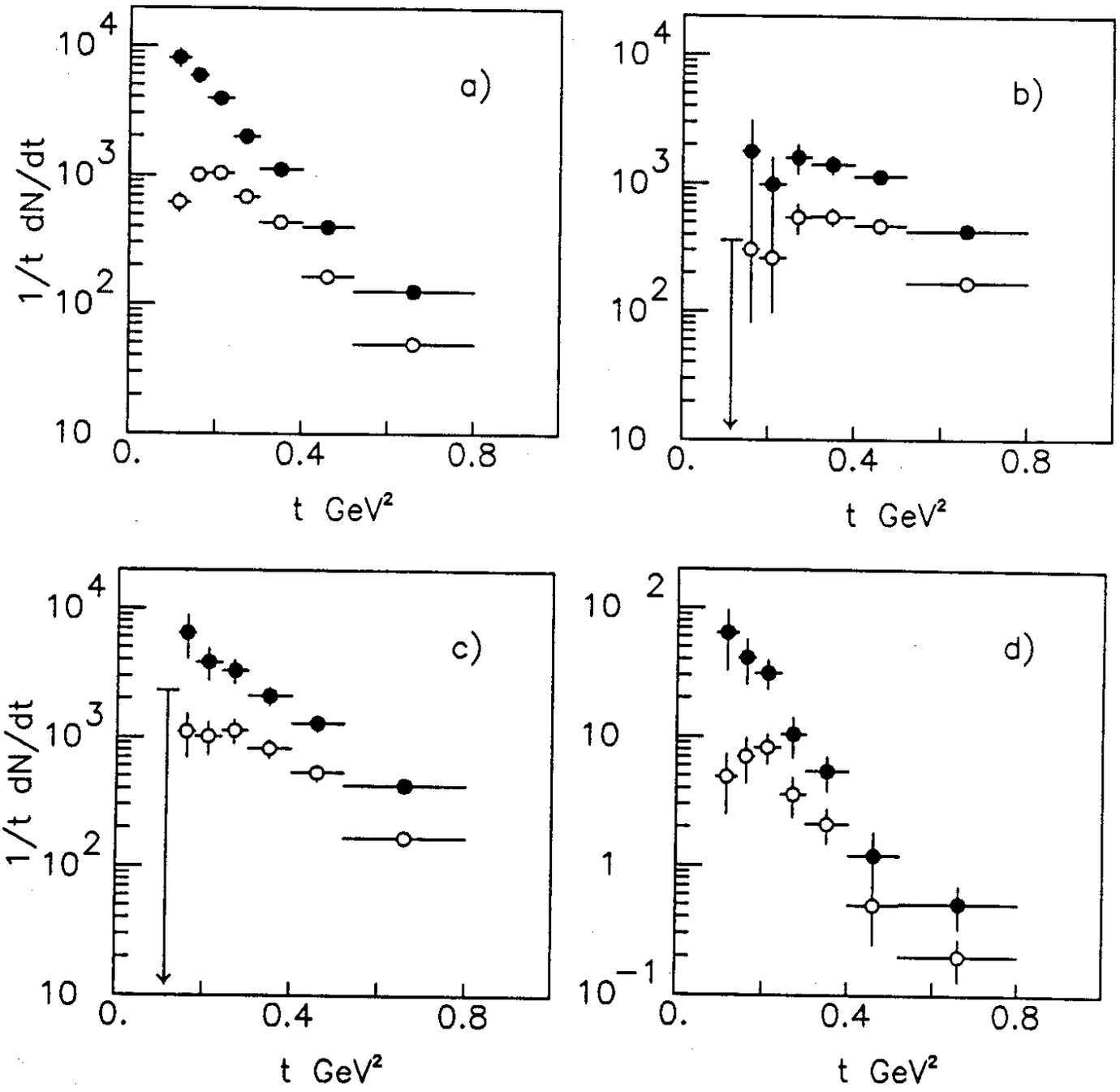

Fig. 17

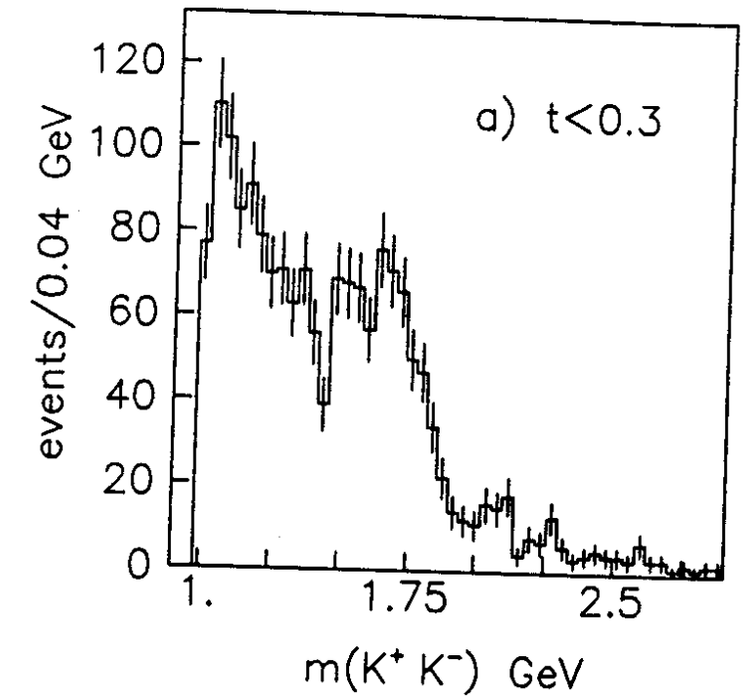
a) t<0.3
events/0.04 GeV
120
100
80
60
40
20
0
1.
1.75
2.5
m(K⁺ K⁻) GeV

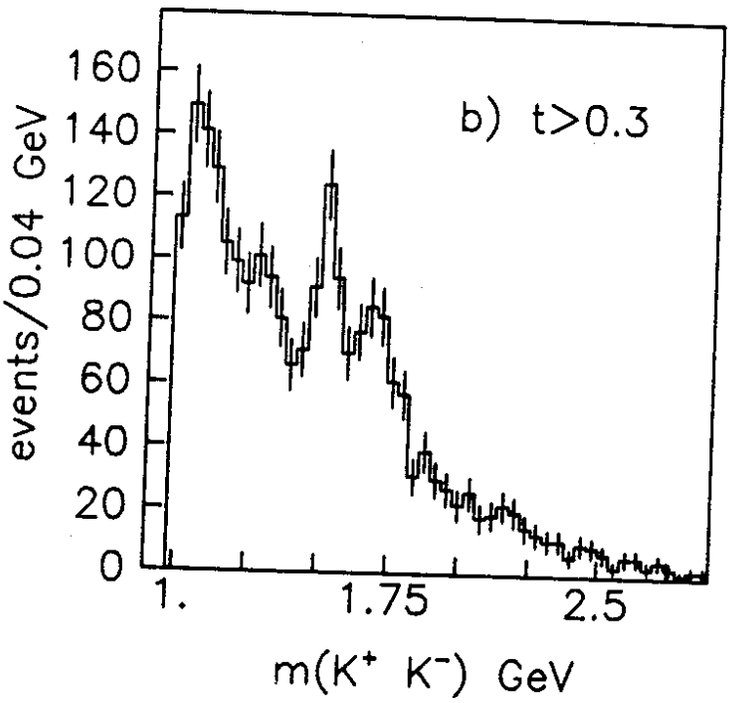
b) t>0.3
events/0.04 GeV
160
140
120
100
80
60
40
20
0
1.
1.75
2.5
m(K⁺ K⁻) GeV

Fig. 18

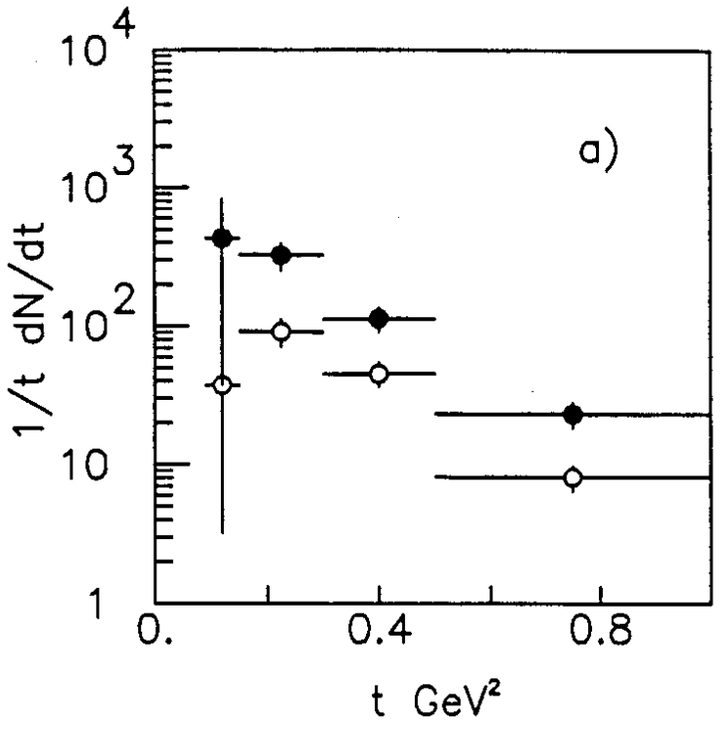
a)
1/t dN/dt
10^4
10^3
10^2
10
1
0.
0.4
0.8
t GeV²

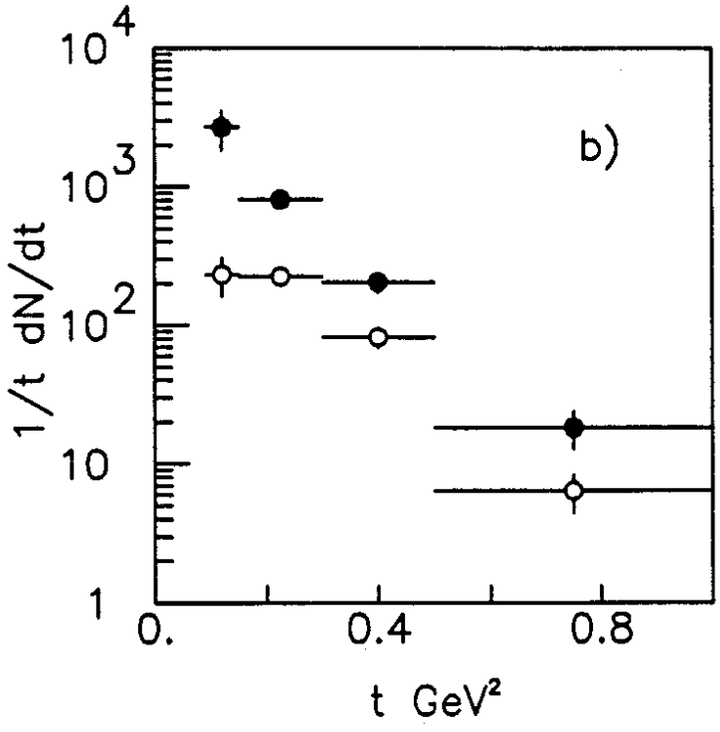
b)
1/t dN/dt
10^4
10^3
10^2
10
1
0.
0.4
0.8
t GeV²

Fig. 19

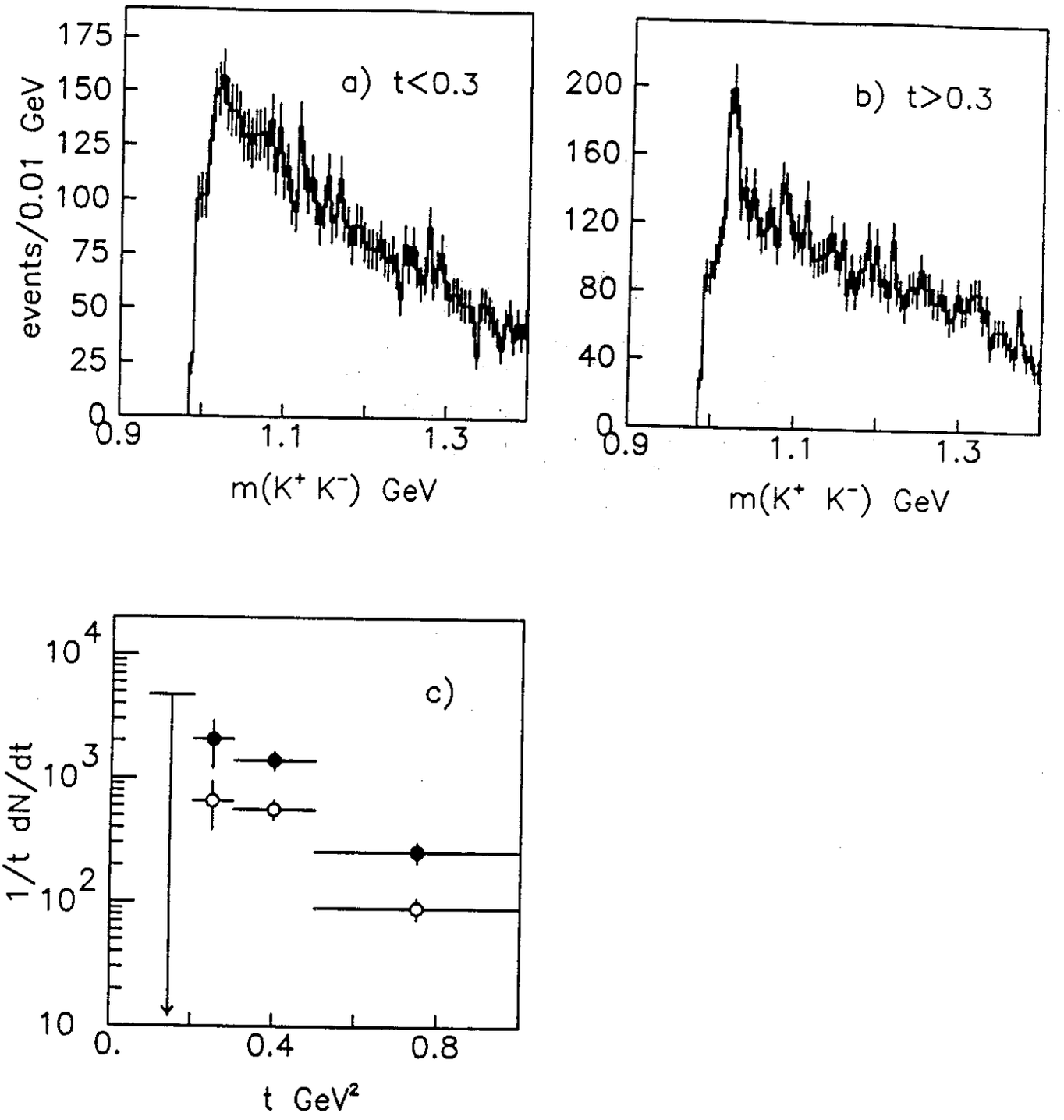

Fig. 20

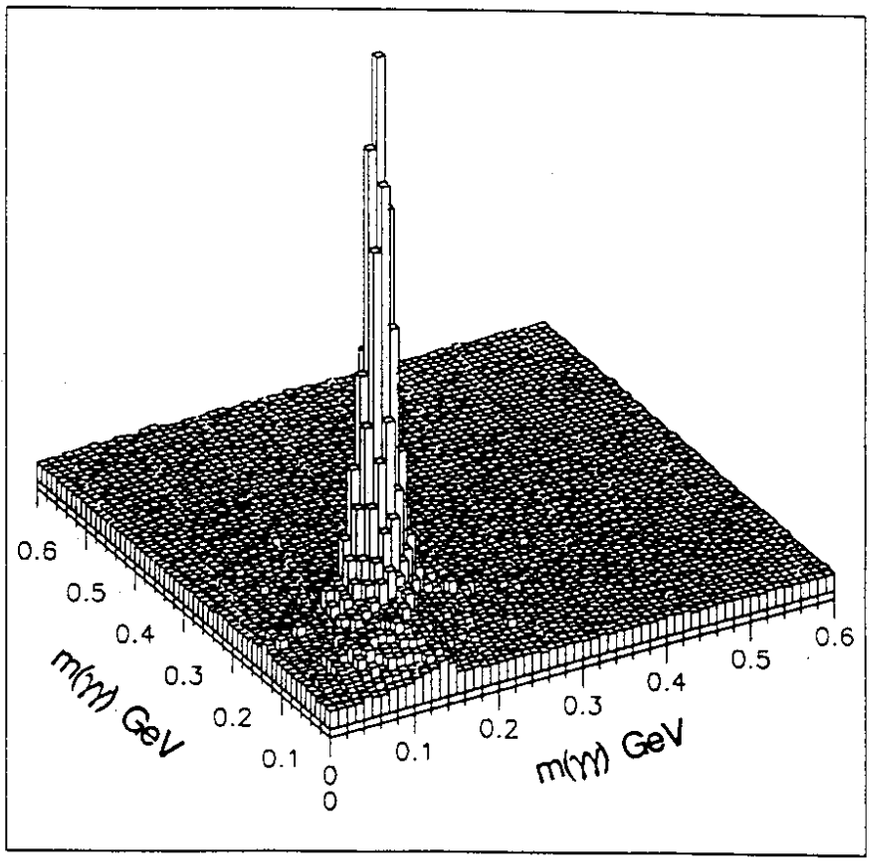

Fig. 21

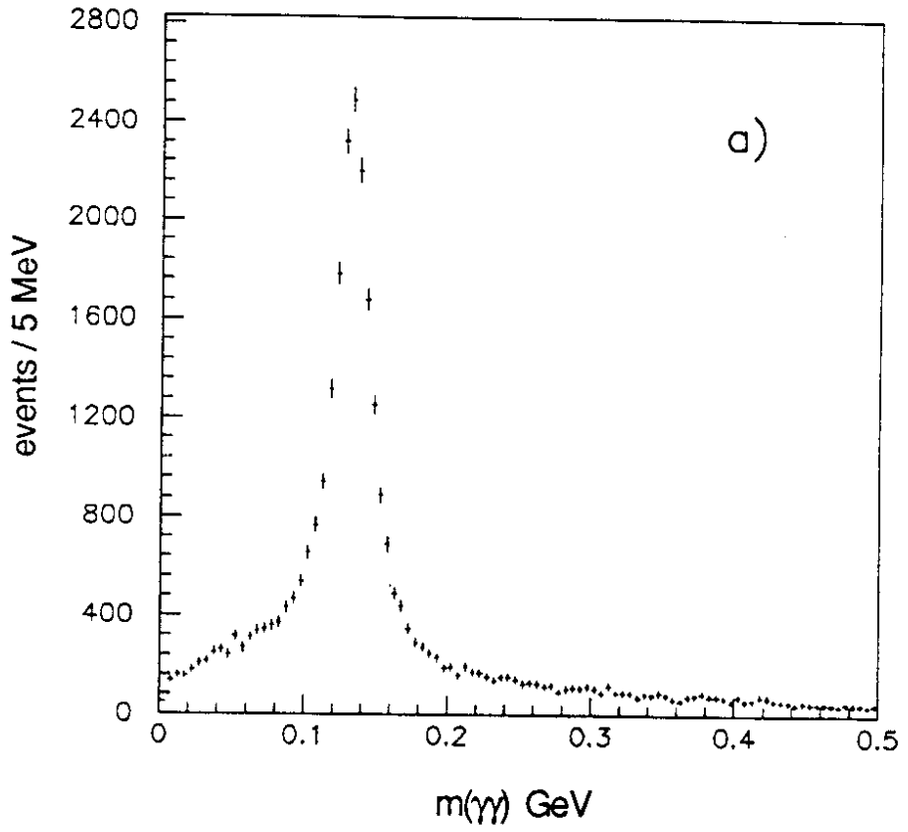
a)
events / 5 MeV
2800
2400
2000
1600
1200
800
400
0
0
0.1
0.2
0.3
0.4
0.5
m(γγ) GeV

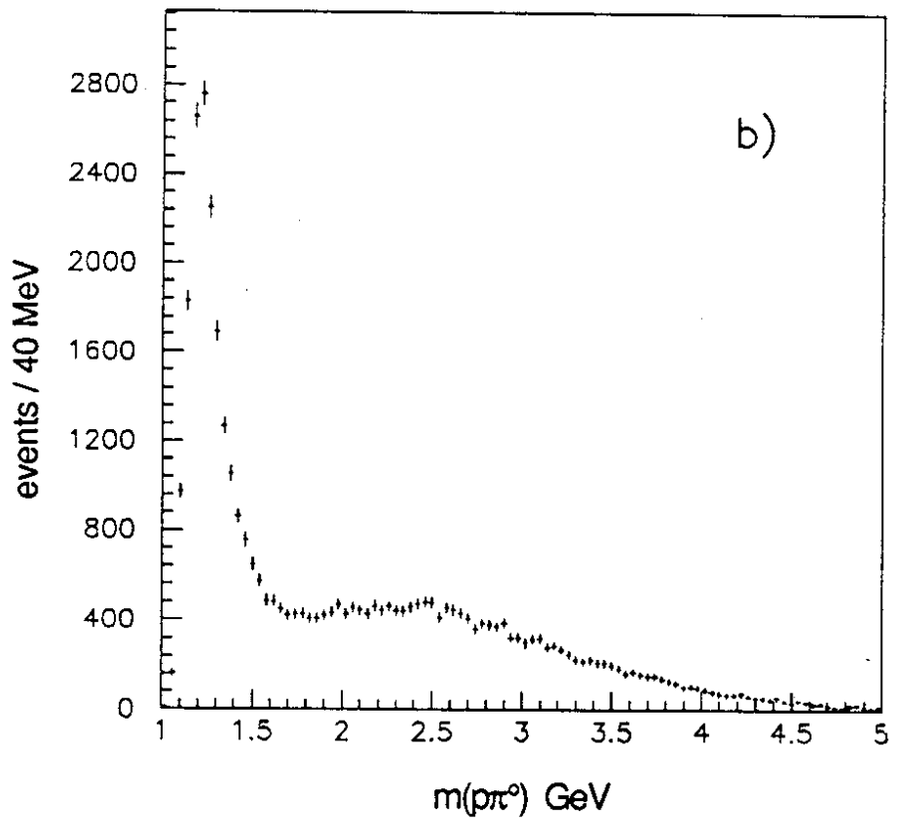
b)
events / 40 MeV
2800
2400
2000
1600
1200
800
400
0
1
1.5
2
2.5
3
3.5
4
4.5
5
m(pπ°) GeV

Fig. 22

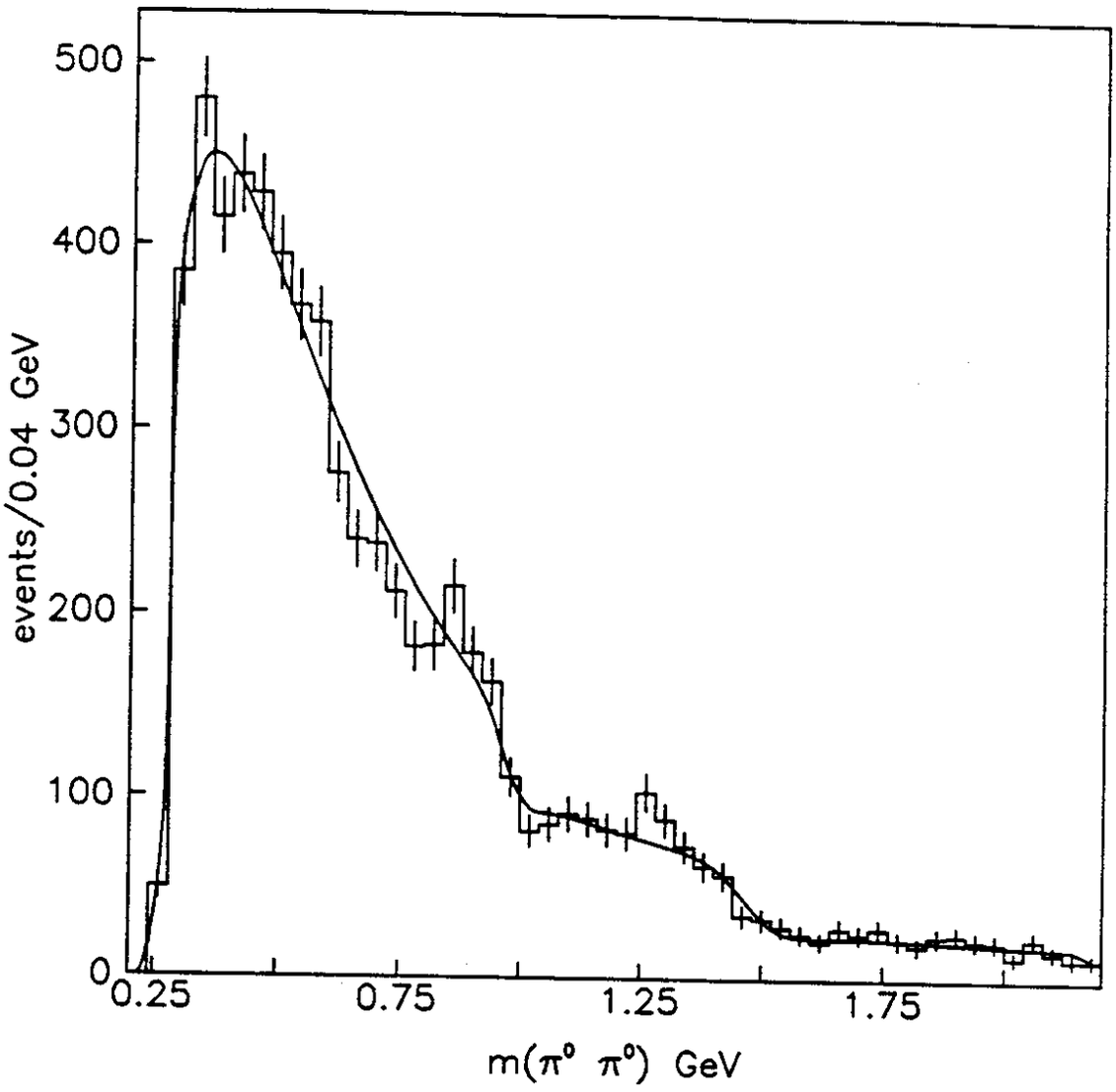

Fig. 23

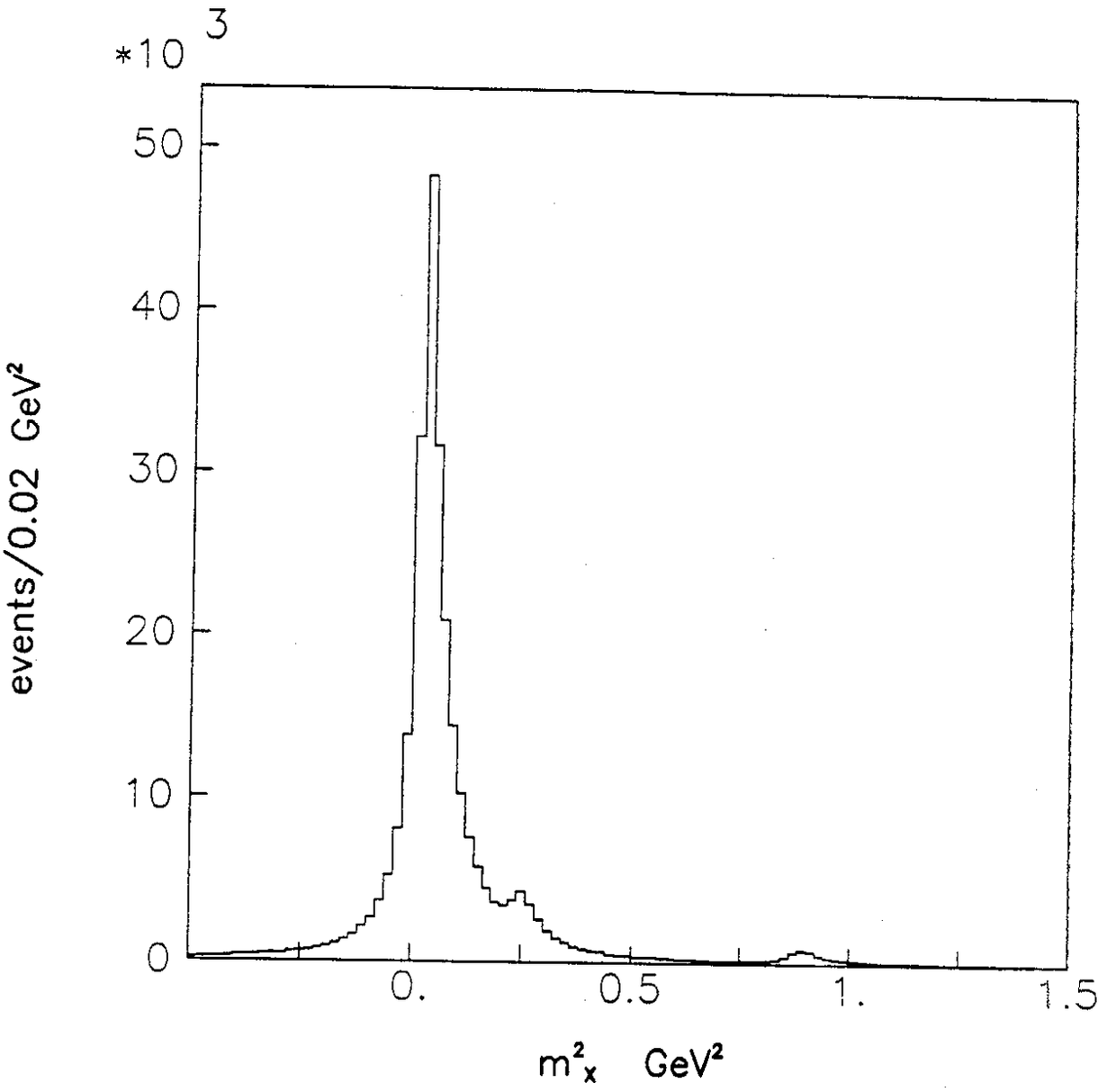

Fig. 24

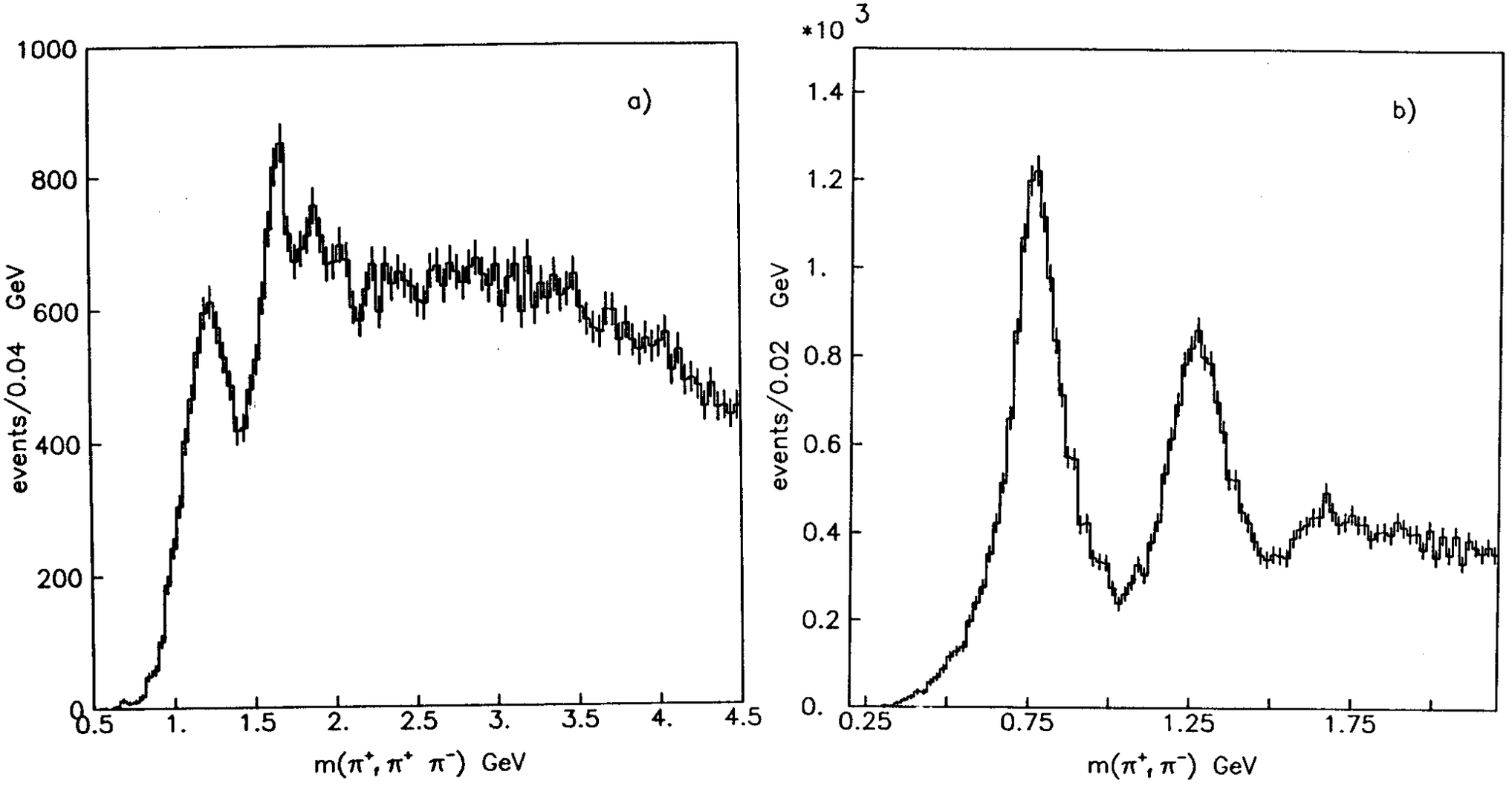
a)
b)
events/0.04 GeV
events/0.02 GeV
*10 3
m(π+, π+ π−) GeV
m(π+, π−) GeV
1000
800
600
400
200
0
1.4
1.2
1.
0.8
0.6
0.4
0.2
0.
0.5
1.
1.5
2.
2.5
3.
3.5
4.
4.5
0.25
0.75
1.25
1.75

Fig. 25

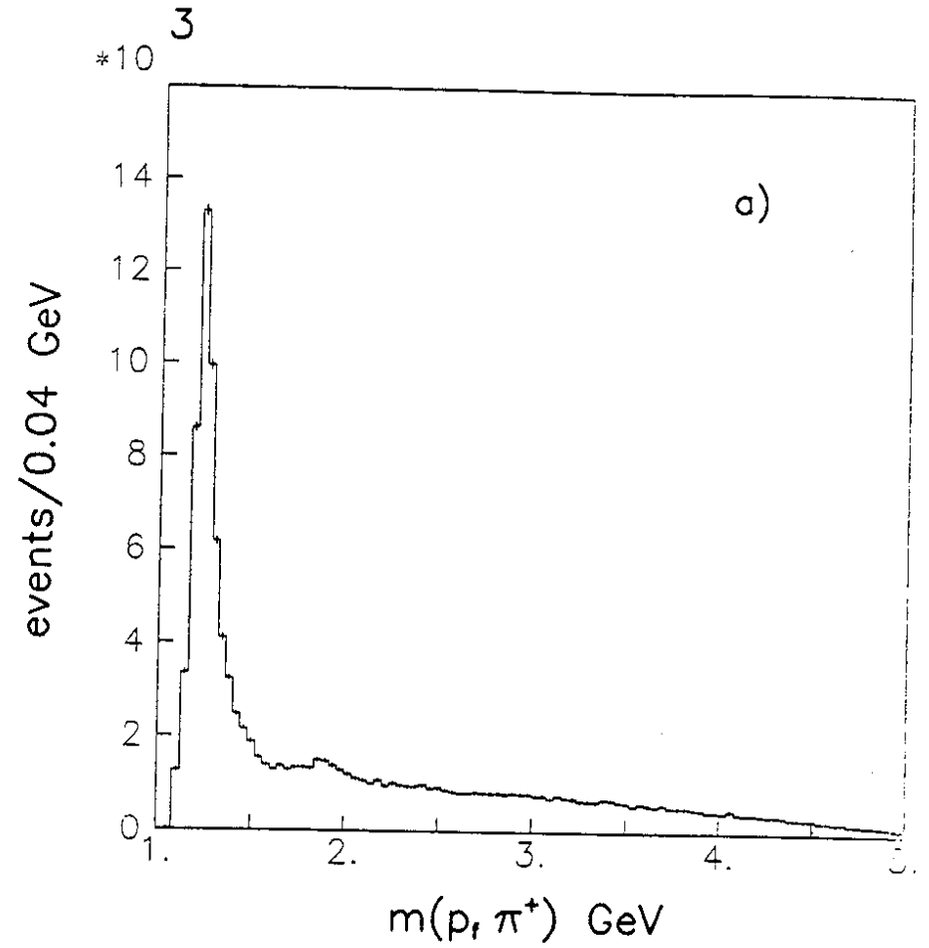
*10 3
14
12
10
8
6
4
2
0
events/0.04 GeV
a)
1.
2.
3.
4.
m(p_f π⁺) GeV

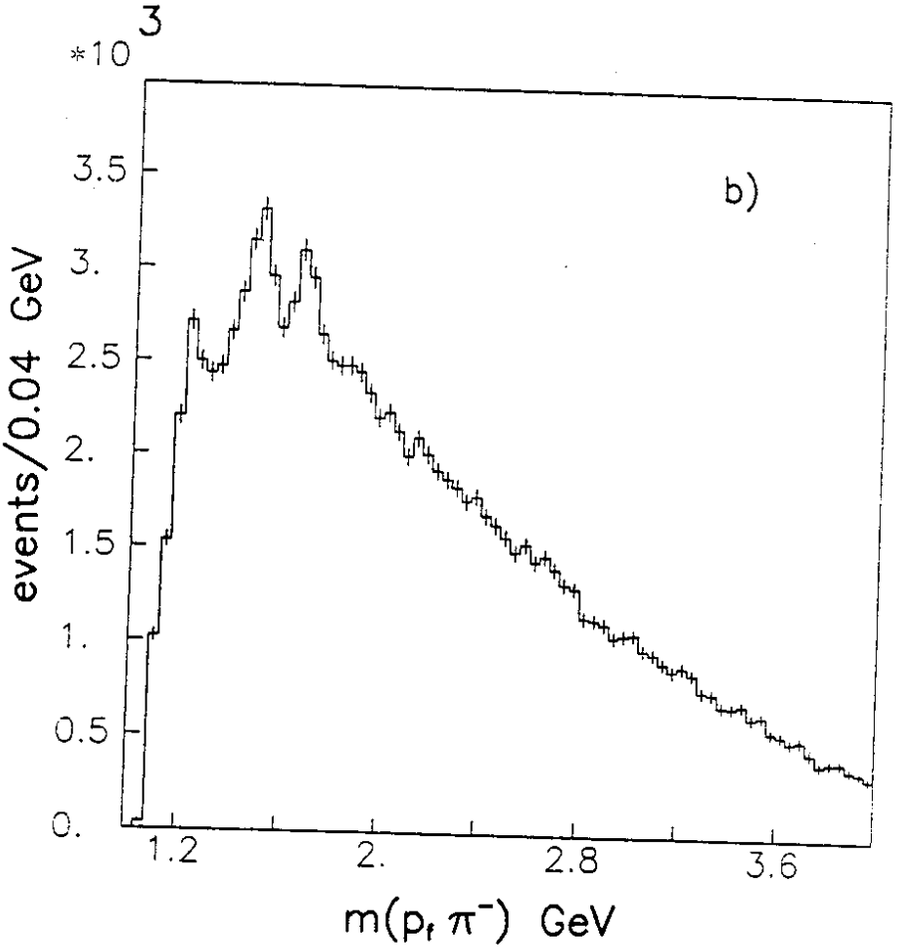
*10 3
3.5
3.
2.5
2.
1.5
1.
0.5
0.
events/0.04 GeV
b)
1.2
2.
2.8
3.6
m(p_f π⁻) GeV

Fig. 26

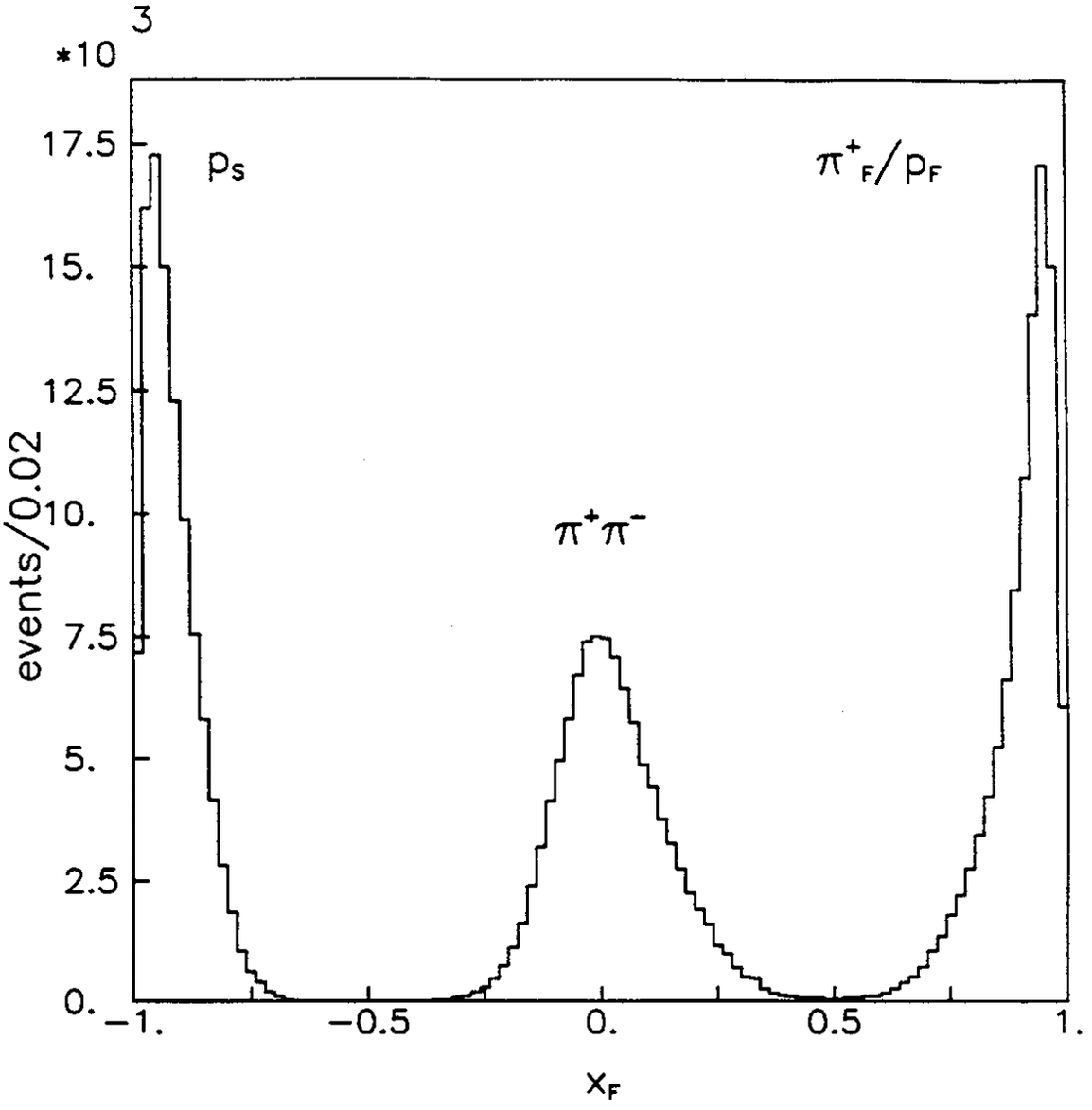

Fig. 27

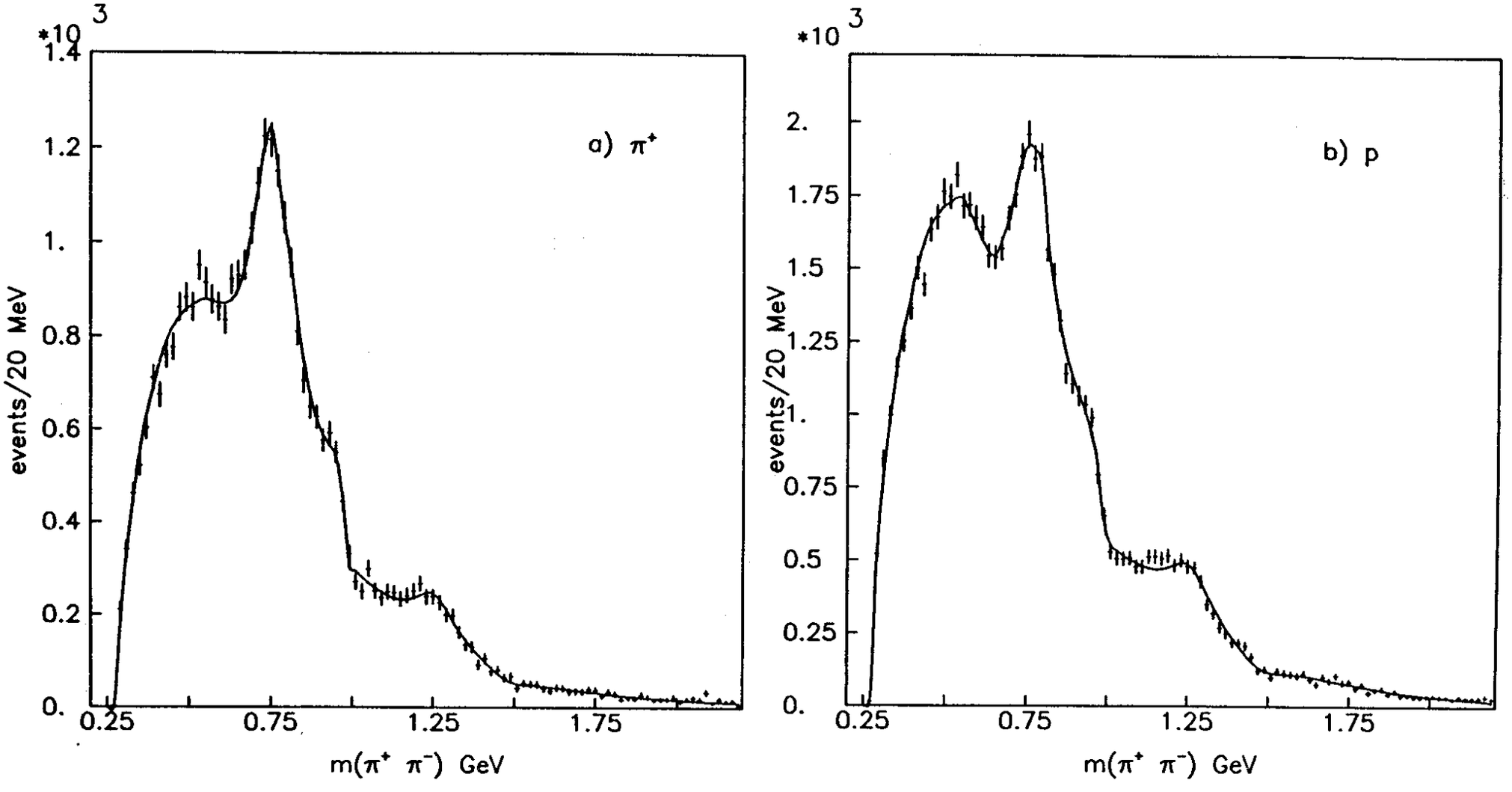
*10 3
1.4
1.2
1.
0.8
0.6
0.4
0.2
0.
events/20 MeV
a) π+
0.25
0.75
1.25
1.75
m(π+ π−) GeV
*10 3
2.
1.75
1.5
1.25
1.
0.75
0.5
0.25
0.
events/20 MeV
b) p
0.25
0.75
1.25
1.75
m(π+ π−) GeV

Fig. 28

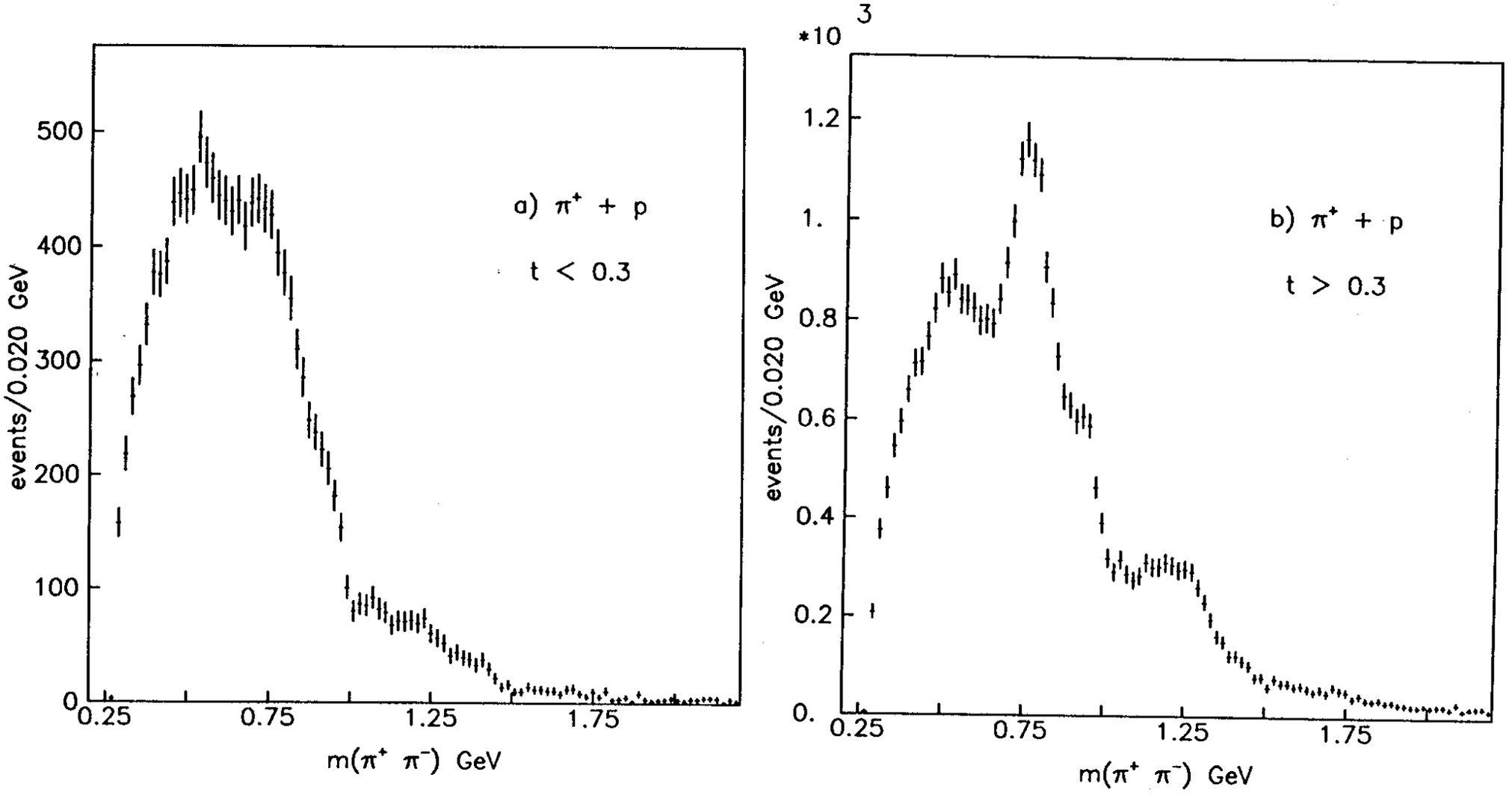
a) π⁺ + p
t < 0.3
events/0.020 GeV
m(π⁺ π⁻) GeV
b) π⁺ + p
t > 0.3
*10 3
events/0.020 GeV
m(π⁺ π⁻) GeV

Fig. 29

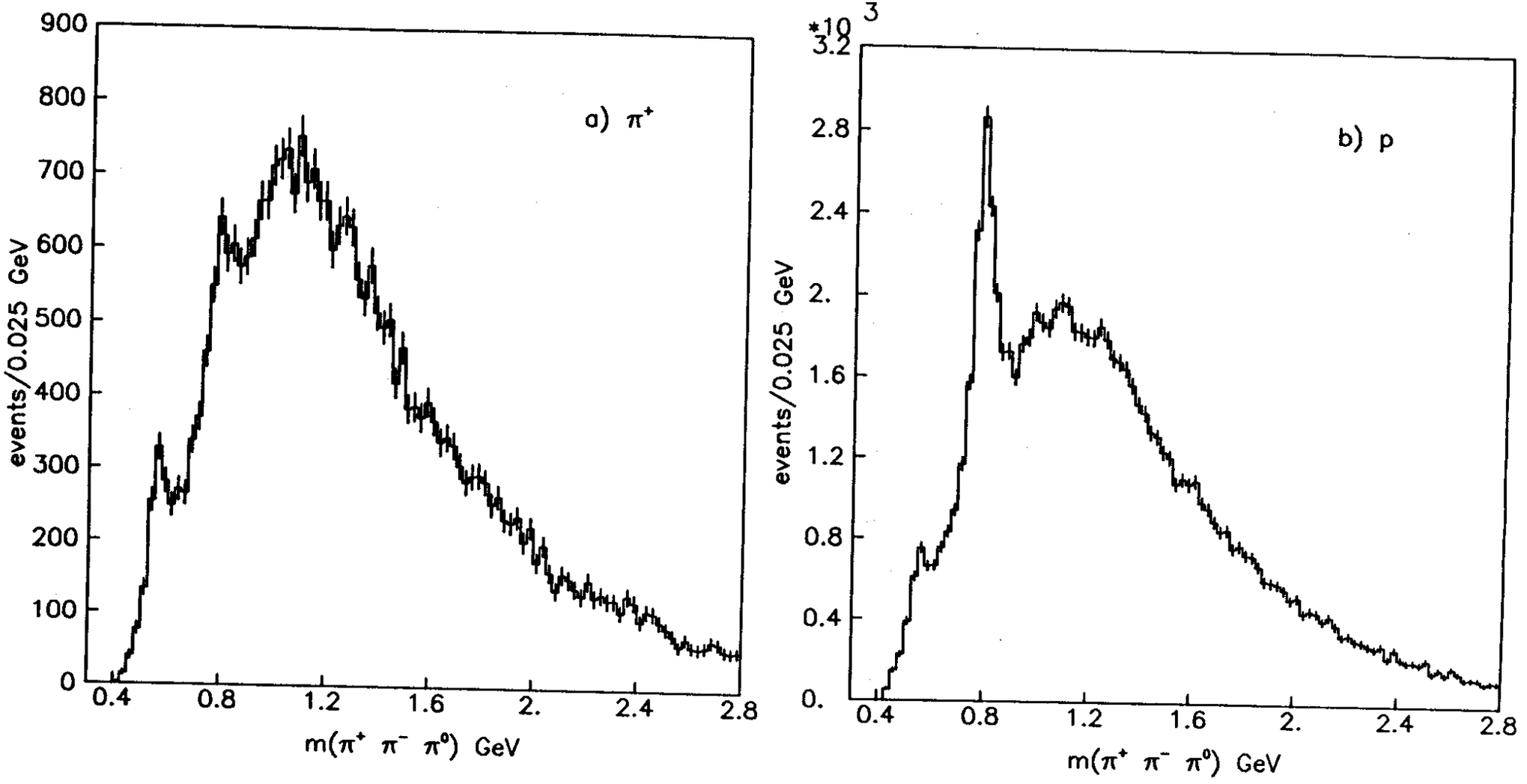

Fig. 30

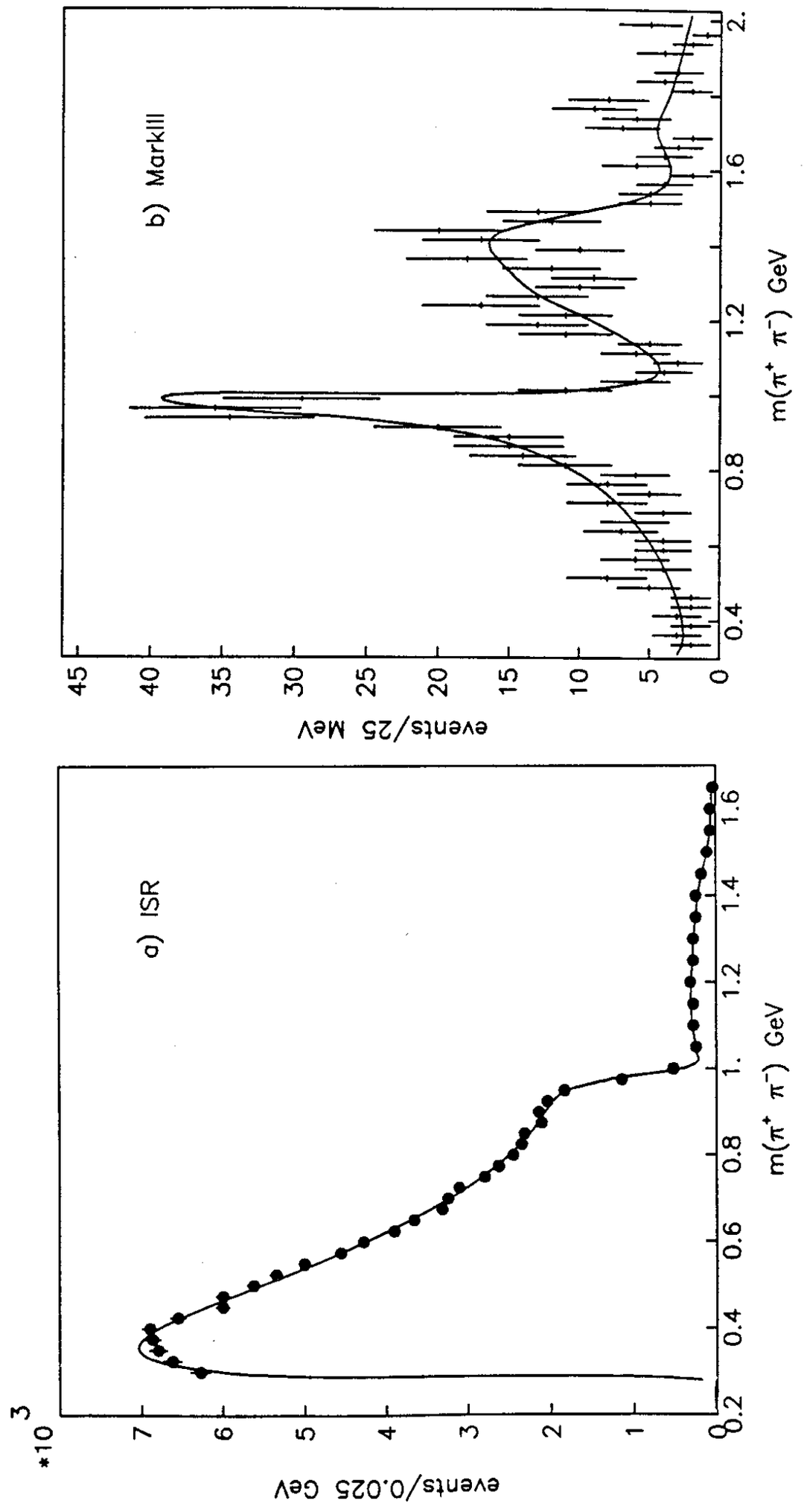

Fig. 31

Imprimé au CERN. Prix : 1.45 Fr.